Coherent exciton transport in semiconductors

19

Massimo Rontani and L. J. Sham

19.1 Introduction

An exciton is a particle-like neutral excitation of solids and molecules composed of one electron and one hole bound together by the mutual electrical attraction [1–5]. Its creation through internal charge separation is most frequently caused by the absorption of light and its demise is occasioned by electron–hole recombination, mostly with emission of light and less frequently non-radiatively. The many-electron ground state of the system, being an insulator, is immune to excitation until the excitation energy reaches a threshold G known as the energy gap. When external influences such as the electromagnetic field and lattice vibrations are ignored, the exciton may be viewed as a robust state of an excited electron plus the hole which has been left behind in the valence electron states [6]. The hole acquires its positive charge from the loss of an electronic charge from the ground state whose total charge is neutralized by that of the ions in the molecule or solid.

The photon–exciton interaction is responsible for the optical excitation (though not necessarily in the visible frequency range) of the exciton and for its spontaneous recombination emitting a photon (a quantum unit of light). The dipole matrix element responsible for the transition between the energy states is strong when the electron and hole wave functions overlap in space or match in wavevector. From Planck's law, the frequency of the emitting light E_X/h is proportional to the energy loss E_X in returning the exciton state back to the ground state, with h being Planck's constant.

If the constituent electron and hole of the exciton are mostly localized at an ion, the exciton is localized, but with some probability to hop from site to site. Such a Frenkel exciton is common in molecules and molecular solids. At the other extreme, if the electron and hole wave functions are widespread as extended orbitals in a molecule or Bloch waves in a crystal, their bound state as the exciton can have their center of mass moving through the system with ease. Such Wannier (or Wannier–Mott) excitons are most common in

broad-band and small-gap semiconductors (a semiconductor is distinguished from an insulator qualitatively by a smaller energy gap, with the frequency of the emitting light from the exciton spanning the range from visible light to very far infrared). Wannier excitons resemble the hydrogen atom or, more closely, the positronium system composed of an electron and a positron. Because of the dielectric screening of the electrical force in small-gap materials and sometimes the small effective mass of the electron, the Wannier exciton radius is 10 to 100 times larger than the positronium radius, which is approximately 0.1 nm.

Excitons, being made of two fermions, behave as bosons on the scale larger than the exciton radius and therefore may macroscopically occupy a single quantum state [7–13]. If the exciton lifetime is long enough to allow for reaching quasi-equilibrium, the dilute and cold gas of optically generated excitons may undergo Bose–Einstein condensation (BEC) [14–16]. The critical temperature for exciton BEC, of the order of 1 K for typical densities in semiconductors, is basically the temperature at which the thermal de Broglie wavelength becomes comparable to the average inter-exciton separation. The possibility of achieving BEC of excitons by shining light on solids has been thoroughly investigated in the last fifty years (see the reviews [15, 17–27]). Semiconductors are particularly appealing for this goal as they may provide excitons with a lifetime (hundreds of ns in bilayer structures [23]) longer than the time required for cooling.

In an indirect-gap semiconductor such as silicon, where the momentum of the exciton does not match that of the photon, the excitons are generally formed after relaxation of optical excitations with initial energy much higher than the gap. The indirect exciton has a long lifetime because its recombination with the emission of a photon requires the conservation of momentum to be satisfied by the assistance of a lattice vibration or trapping by a defect. Consequently, the excitons have time to form a large pool known as an electron–hole drop (see the reviews [28, 29]). Alternatively, the delay in optical recombination may be due to the symmetry of the crystal, as in the direct-gap oxide Cu_2O which has conduction and valence bands of like parity hence the optical dipolar transition is forbidden [30]. The chapter by Kuwata–Gonokami in Volume 1 focuses on the aspects of BEC of optically generated excitons in semiconductors.

In a direct-gap material, the spatial separation of the electron and hole can be enforced by housing them in two layers sufficiently close to maintain their electric attraction [31–33]. The recombination of such indirect excitons may then be controlled by changing the electron and hole wave function overlap with an electric field [34, 35]. An interesting phenomenon is the laser spot excitation of these indirect excitons, leading to the formation of two concentric luminous circles centered at the laser spot plus other localized bright spots randomly placed between the circles. Whereas the formation of the inner ring [36] is due to the migration of indirect excitons away from the laser spot as optically inactive excitons, the localized bright spots [36] as well as the outer ring [36–39] form on the boundaries between electron-rich and hole-rich regions. At low temperature the outer ring is a necklace of evenly spaced bright spots, whose origin is not fully understood [40]. This system of excitons in a double quantum

well is considered a good candidate for condensation. These experiments and related work in double quantum wells are reviewed in [22–26, 41].

Another possible—and elusive—mechanism of condensation of excitons as bosons is that excitons form spontaneously at thermodynamic equilibrium even in the absence of an optical excitation. Such process signals the transition to a permanent phase known as excitonic insulator (EI) [1, 42–45], which is originated by the instability of the normal ground state of either a semiconductor or a semimetal against the spontaneous formation of bound electron–hole pairs. The wave function of the strongly correlated EI ground state is formally similar to that proposed by Bardeen, Cooper, and Schrieffer for superconductors [46]. As a matter of fact, both excitons and Cooper pairs are absent except as fluctuations in the normal high-temperature phase and form only in the ordered, low-temperature phase—respectively the EI and the superconductor. Besides, both condensation of excitons and that of Cooper pairs are best described in the reciprocal space of the crystal solid. The EI phase is reviewed in [14, 15, 17, 19, 20, 22, 26, 27, 47–50].

It is intriguing to observe that condensation of other types of bosons composed of two fermions leads to spectacular manifestations of quantum mechanical coherence, such as the superfluidity ensuing from the pairing of ^{3}He atoms [51], Fermi alkali atoms confined in optical traps [52, 53], nucleons in neutron stars [54, 55], the superconductivity induced by Cooper pairs in metals [56], and the non-classical momenta of inertia in nuclei [57, 58]. The above phenomena may regarded as distinct realizations of superfluidity, associated to the coherent, dissipationless flow of charge and/or mass. However, excitons are neutral and stay dark unless recombine radiatively, as shown in Table 19.1, which compares the distinct features of the condensates made of composite bosons. The signature of the macroscopic order of the exciton condensate is, at present, controversial for the superfluid transport but its other manifestations will be discussed next.

The aim of this chapter is to illustrate some recent theoretical proposals concerning the detection of coherent exciton flow [59–61]. The reader may refer to the literature reviewed in Section 19.2 for a discussion of the conceptual and experimental difficulties inherent in the realization of exciton condensates. Here we set aside such difficulties and adopt in a pedagogical way the simplest mean-field description of the condensate, on which we lay our theoretical development in order to detect the transport properties of the exciton condensate.

In particular, we focus on the exciton analogues of two phenomena, i.e., Andreev reflection and Josephson effect, which are hallmarks of superconducting behavior, and stress the crucial differences between excitons and Cooper pairs. Our first main conclusion is that the excitonic insulator is the *perfect* insulator in terms of both charge and heat transport, with an unusually high resistance at the interface with a semimetal—the normal phase of the condensed state. Such behavior, which should be contrasted with the high electrical conductance of the junction between superconductor and normal metal, may be explained in terms of the coherence induced into the semimetal by the proximity of the exciton condensate. Then we show that the exciton superflow

Table 19.1 Excitonic insulator (EI) versus superconductor *à la* Bardeen–Cooper–Schrieffer (BCS). The interface referred to in the table is the junction between normal and condensed phase. For a general discussion of the condensates made of composite bosons see [62]. For specific EI features see [45] (Meissner effect), [63] (superconductivity), [64] (superthermal conductivity), [59, 60] (Andreev reflection), and [61] (Josephson oscillations).

Physical property	Excitonic insulator	BCS-like superconductor
Nature of the composite boson	Exciton	Cooper pair
Boson charge	Neutral	$2e$
Boson momentum	Crystal momentum	Crystal momentum (commonly ignored in the free electron gas approximation)
Boson mass	Effective mass	Effective mass of the electron quasiparticle in the Fermi level region (of thickness provided by phonon Debye frequency)
Type of long-range order	Diagonal	Off-diagonal
Superfluidity	?	Superconductivity
Meissner effect	No	Yes
Superthermal conductivity	No	No
Nature of the quasiparticle	Electron (hole)	Bogoliubon
Andreev reflection	Yes	Yes
Interface electric conductance	Decreased	Increased
Interface thermal conductance	Decreased	Decreased
Proximity effect	Yes	Yes
Josephson oscillations	Yes	Yes

may be directly probed in the case that excitons are optically pumped in a double-layer semiconductor heterostructure: we propose a correlated photon counting experiment for coupled electrostatic exciton traps which is a variation of Young's double-slit experiment.

We last mention that, due to the interaction between electrons and light, not only can an exciton decay irreversibly into a photon or vice versa, but it can also exchange roles with the photon in a quantum-mechanically coherent fashion. Thus, the exciton may exist in the solid in the superposition state of an exciton and a photon, known as polariton. Whereas the photon energy varies linearly with its momentum at the speed of light in the vacuum, the exciton energy depends on the square of its center-of-mass momentum. For small momenta, the exciton and the photon can approximately match both their momentum and energy values, the coupling mixing the two states into two superpositions of photon and exciton with an energy splitting. Thus, the massless photon is slowed down by the massive exciton by virtue of the quantum-mechanical superposition. The chapter by Yamamoto in Volume 1 deals with aspects of polariton condensation.

The structure of this Chapter is the following: After a review of previous work (Section 19.2), in Section 19.3 we illustrate the mean-field theory of the EI emphasizing its relation with the BCS theory of superconductors. We then introduce the phenomenon of Andreev reflection in Section 19.4 and analyze its observable consequences in Section 19.5. Section 19.6 on the Josephson effect ends the chapter.

19.2 Physical systems

This section briefly reviews recent theoretical and experimental works on exciton condensation, focusing on diverse physical systems. Without attempting an exhaustive review, we refer the reader to more comprehensive essays whenever available.

19.2.1 Bose–Einstein condensation of optically generated excitons

The pursuit of Bose–Einstein condensation of optically generated excitons in semiconductors, which dates back to the sixties, presently focuses on both classic systems such as Cu_2O and novel low dimensional structures (for reviews see [15, 17–27, 41, 50, 65–67]). A very active field concerns "indirect" excitons. Such excitons are made of spatially separated electrons and holes, hosted in two quantum wells that are sufficiently close to maintain electrical attraction between the carriers of opposite charge. This setup has several advantages: (i) The overlap of electron and hole wave functions is controlled by applying an electric field along the growth direction of the bilayer heterostructure, thus increasing the exciton recombination time by orders of magnitude with respect to the single-well value [34, 35]. (ii) The confinement effect along the growth direction increases the exciton–phonon scattering rate, improving exciton thermalization [68]. (iii) The dipolar repulsion among indirect excitons disfavors the formation of biexcitons and electron–hole droplets [50, 69–75] as well as effectively screens the in-plane disorder potential [76–81]. (iv) As the electric field parallel to the growth direction may be laterally varied using suitably located electrodes, one may tailor the in-plane effective potentials for excitons, thus realizing artificially controlled traps [78, 79, 81–89], ramps [90, 91], lattices [80, 92–94], "exciton circuits" [95–97], and "exciton conveyers" [98].

Exciton traps may also be created by means of the uncontrolled in-plane disorder of the double quantum well [36, 78, 79, 99, 100], the strain experienced by the heterostructure [101–106], the laser-induced confinement [107, 108], the magnetic field [109]. The realization and control of exciton traps is a key capability to reach exciton BEC: as the long range order in two dimensions is smeared by quantum fluctuations, a weaker requirement for the macroscopic occupation of the lowest exciton level is that the exciton coherence length exceeds the trap size [24].

The present evidence of exciton BEC is based on distinct features of the emitted light (photoluminescence, PL) that appear at low temperature: (i) The PL dynamics exhibits bosonic stimulation of the scattering of hot optically dark excitons into optically active low-energy states [110]. (ii) The PL signal becomes noisy in a broad range of frequencies, as it occurs in the presence of coherence [69, 111, 112]. (iii) The degree of polarization of the emitted light increases with decreasing temperature [40, 113, 114], consistently with gauge symmetry breaking. (iv) The exciton mobility is enhanced, which may be attributed to superfluid behavior [115]. (v) The radiative decay rate increases, which may be explained in terms of "superradiance" of a macroscopic dipole [115] or collective behavior at the onset of condensation [113, 114]. (vi) The

PL lineshape narrows and departs from the Maxwell–Boltzmann distribution [111, 113, 114, 116], as it may be expected for the macroscopic population of a single exciton state.

However, some of the signatures [30, 117–119] listed above, taken separately, may have different explanations than exciton condensation [120–122] (for a discussion see [24]). The most compelling evidence of BEC is probably the direct measure of coherence through interferometric techniques [40, 41, 88, 123–126], which accesses the macroscopic exciton wave function in real space. On the theory side, the light emitted by excitons just after the onset of condensation is predicted to be coherent [127–129], with a sharply focused peak of radiation in the direction normal to the quantum-well plane [130, 131]. Besides, the instability leading to the external ring of evenly placed bright spots discussed in the introduction [36, 38] is possibly linked to exciton quantum degeneracy [132].

An intriguing issue is the role played by spin [133] in exciton condensation. In bilayers, the exciton spin is the component J_z of the angular momentum along the direction perpendicular to the planes, discriminating between optically active ($J_z = \pm\hbar$) and inactive states ($J_z = \pm 2\hbar$). The most urgent questions concern the multicomponent nature of the condensate [134, 135], the possibility of dark-exciton condensation [136, 137], the role of spin-orbit coupling [138–141]. This research is fueled by the recent experimental evidence that the spin-relaxation time of indirect exciton is long and consequently exciton spin transport is long-ranged [142, 143], as well as that spin textures and polarization vortices appear together with the onset of long-range coherence [40].

19.2.2 Excitonic insulator in mixed-valence semiconductors

In principle, any intrinsic semiconductor that may be turned into a semimetal, either by applying stress or by suitable alloying, may undergo a transition to the permanent EI phase. Favorable conditions are the presence of an indirect gap, which weakens the detrimental effect of dielectric screening on the exciton binding, as well as the nesting of electron and hole Fermi surfaces, which maximizes electron–hole pairing. Nevertheless, early experiments focusing on simple materials, such as divalent fcc metals (Ca, Sr, Yb) and group V semimetals (As, Sb, Bi) were unable to confirm the existence of the EI. References [14, 15, 17, 19, 20, 26, 47–50] review the work on the EI.

Recently, a few experiments have pointed to the realization of the EI phase in mixed-valent semiconductors. The first class of candidate materials consists in rare-earth chalcogenides, such as $TmSe_xTe_{1-x}$ [144, 145], $Sm_{1-x}La_xS$ [145, 146], $Sm_{1-x}Tm_xS$, YbO, and YbS [146]. These compounds all crystallize in the NaCl structure and undergo a semiconductor–semimetal transition as the band gap G is changed from positive to negative values by applying high hydrostatic pressure to the sample.

When the direct gap of $TmSe_{0.45}Te_{0.55}$, formed between the localized $4f^{13}$ levels and the $5d$ conduction-band states, is closing with external pressure, an

indirect band gap develops between the highest valence Tm $4f^{13}$ level Γ_{15} at the Γ point and the minimum of the $\Delta_{2'}$ conduction band $5d$ states at the X point of the Brillouin zone. As the otherwise localized $4f$ band is broadened and shows a maximum at Γ due to p(Se,Te)–f(Tm) covalent hybridization [147], it is tempting to use a simple two-band model for interpretation, similar to the one illustrated in Section 19.3. On the basis of low-temperature resistivity and Hall mobility measurements, the authors of [144] attribute the resistivity increase with the vanishing gap to a condensation of free carriers into excitons, placing the EI phase between semimetal and semiconductor, close to $G \approx 0$. Later, the same group has reported a linear increase of thermal conductivity and diffusivity with decreasing temperature and attributed it to exciton superfluidity [148]. Fehske and coworkers [149–151] have suggested theoretically that the EI phase in the pressure-temperature phase diagram is narrower that the experimental claim, being surrounded by a "halo" regions made of preformed excitons coexisting with the normal semiconductor phase. The presence of this halo, precursor of the EI, explains the experimental findings and rules out the idea of a heat supercurrent, which conflicts with the general argument [45, 64] that a flowing condensate carries no entropy and thus no heat.

Other candidate systems for the EI phase are the transition metal chalcogenides $TiSe_2$ [152–166], Ta_2NiSe_5 [167], $TaSe_2$ [168], and the possibly ferromagnetic EI GdI_2 [169, 170] (see [171] for a review). The main evidence relies on the hole quasiparticle band structure, as extracted from angular-resolved photoemission [154–162, 165, 167]. The much studied $TiSe_2$, at a critical temperature of around 200 K, develops a charge density wave [152] which does not fit the standard model based on Fermi surface nesting [171, 172] but it is consistent with the presence of an EI (see Section 19.3). In fact, the spanning wavevector of the charge density wave is the distance in reciprocal space between Ti $3d$-electrons and Se $4p$-holes, which are bound by Coulomb attraction. Therefore, the excitonic instability drives the charge density wave and may possibly couple with a periodic lattice distortion [156, 158, 160, 162, 164–166], though alternate scenarios [159, 163, 171] have been suggested. Recent time-resolved photoemission data link the artificially induced collapse of the charge-ordered $TiSe_2$ state to screening due to transient generation of free charge carriers, supporting the excitonic origin of the phase transition [173, 174].

A third class of candidate systems consists in Kondo insulators [175] and heavy-fermion materials [176], which are mixed-valence semiconductors characterized by a flat f-type valence band plus a dispersive—say d-type—conduction band, typically exhibiting strongly correlated behavior. Such systems (e.g., SmB_6) are often modeled by the Falicov–Kimball hamiltonian, which takes into account the strong inter-band Coulomb interaction [177–180]. Sham and coworkers have shown [178, 181] that the exciton condensate made of f holes and d electrons may spontaneously break the lattice inversion symmetry and lead to a ferroelectric phase transition of electronic origin, whereas conventional ferroelectricity is associated to lattice distortion [182]. The predicted experimental signatures, supported by some evidence [183, 184], include the divergence of the static dielectric constant, a ferroelectric resonance in the microwave absorption spectrum, and a non-vanishing susceptibility for second-harmonic generation.

If intraband hybridization dominates over Coulomb interaction, then the exciton condensate wave function acquires a different type of symmetry—p-wave—which excludes the ferroelectric scenario but allows the coupling with the lattice [185]. In this latter case the excitonic instability manifests itself as a spontaneous lattice deformation which may explain some of the phase transitions known as ferroelastic [186].

19.2.3 Permanent exciton condensation in bilayers

In order to investigate permanent exciton condensation in semiconductor bilayers, one strategy is to host electrons in the first layer and holes in the second layer [31, 32]. This task is nowadays accomplished by means of suitable electric gates which allow to separately contact the layers [187–192]. The spacer between the two quantum wells suppresses the inter-layer tunneling which induces exciton recombination, but it is sufficiently thin to provide strong inter-layer Coulomb interaction (see [193] for a recent review). This setup allows for measuring the Coulomb drag resistance, which is the inverse ratio of the electric current measured in one layer to the open-circuit voltage developed in the other layer in turn. Such drag resistance is predicted to diverge in the presence of exciton condensation, as the exciton binding correlates the motion of carriers in the two layers [194–196]. Recent measurements [197–199] point to low-temperature anomalies in the Coulomb drag which may originate from an excitonic instability, though other strongly correlated phases are possible [193].

An alternate strategy is to place electrons in both layers in the presence of the magnetic field (see [200–202] for reviews). The field bends classical electron trajectories into circular cyclotron orbits. As such orbits may be placed all across the plane, overall their quantized energies consist in highly degenerate "Landau levels". Since the level degeneracy is the number of quanta of magnetic flux that cross the plane, for sufficiently high fields and identical layers the lowest Landau level in each layer will be half filled by electrons (single layer filling factor $\nu = 1/2$, total filling factor $\nu_T = 1$). Note that in this quantum Hall effect regime, routinely detected through the quantization of the Hall resistance, Landau levels may be considered either half filled or half empty. Therefore, one may switch to the excitonic parlance [203, 204], regarding one layer as filled by electrons and the other one by holes. In this picture the exciton "vacuum" has the lowest Landau level totally filled in one layer ($\nu = 1$) and empty in the other layer ($\nu = 0$), thus excitons are created by moving electrons from one layer, which leaves a hole behind, to the other one [205].

There is significant evidence, based on low-temperature transport experiments, that the bilayer ground state is a condensate of excitons. The first hint is a huge enhancement of inter-layer tunneling solely due to many-body effects, clearly pointing to strong inter-layer coherence [206]. The most compelling observations are based on counterflow measurements [31, 32, 207], where the electric currents of opposite sign and like magnitude that flow in the two layers provide zero total electric current and a net exciton flow. For filling factors other than ν_T=1 the Hall voltages separately measured in the two layers are equal and opposite in sign, whereas for ν_T=1 they both drop

to zero, consistently with the flow of an uncharged object such an exciton [208–210]. To prevent edge states—always present at the boundary of quantum Hall systems and unrelated to excitons—from playing a role in transport, the Coulomb drag has been recently measured in the "Corbino" annular geometry, confirming the excitonic nature of transport [211–214], whereas the superfluid character of the exciton flow is unclear. The above scenario is supported by the measurement of quasiparticle and collective excitations by means of tunneling [215, 216] and inelastic light scattering [217, 218] spectroscopies.

Interesting theoretical predictions concern the response of the bilayer exciton condensate to external electromagnetic fields [196, 219–221] and impurities [222], as well as the transport properties of hybrid circuits including exciton condensates and superconductors [223–225]. For weak inter-layer interaction or filling factors other than $\nu_T = 1$, bilayers are predicted to undergo phase transitions to other strongly correlated phases, such as paired two-dimensional Laughlin liquids and Wigner solids [204], or peculiar excitonic charge density waves [226].

19.2.4 Graphene-based systems

Graphene—a recently discovered allotrope of sp^2 bonded carbon—is a one-atom thick two-dimensional honeycomb lattice [227–230]. Its peculiar electrical and mechanical properties—chemical stability, high mobility, easiness of making electric contacts—have stimulated observations by means of different electron spectroscopies and scanning probes. Intensive investigations have uncovered new physics (e.g., Klein tunneling, anomalous types of quantum Hall effect), rooted in the unusual character of quasiparticle excitations, that, in the neighborhood of the Fermi energy, are massless chiral Dirac fermions. In fact, conduction and valence bands form specular cones whose apexes touch in the two inequivalent points K and K′, located at the corners of the hexagonal two-dimensional Brillouin zone. These two points, which map into each other by a rotation of $2\pi/6$ [231], are the Fermi surface of the undoped system, hence graphene is a zero-overlap semimetal.

In principle, graphene is a good candidate system for EI, since: (i) the density of states vanishes at the charge neutrality point, hence the long-range Coulomb interaction is unscreened (ii) the perfect electron–hole symmetry of Dirac cones favors the nesting of electron and hole isoenergetic surfaces. Khveshchenko [232] was the first to suggest that graphene hides a latent excitonic insulator instability. The EI phase is a charge density wave alternating between the two inequivalent triangular sublattices, its spamming wavevector connecting K and K′ in reciprocal space. A stack of graphite layers in a staggered (ABAB . . .) configuration, with the atoms located in the centers and corners of the hexagons in two adjacent layers, respectively, could stabilize the EI by enforcing interlayer Coulomb interaction.

After this seminal prediction, many theoretical works have tried to estimate the size of the EI transport gap as well as the stability of the EI phase (see, for example, [233–237] and references therein as well as the reviews [230, 238, 239]). The absence of consensus is not surprising, as the many-body

problem in graphene is presently an open issue [230, 240]. Experiments show that electrons in graphene allegedly behave as non-interacting particles [227–229], except for small effects related to velocity renormalization [241], coupling with phonons [227–229] / plasmons [242] (here we are not concerned with the fractional quantum Hall effect [243, 244], induced by the magnetic field). Therefore, if the EI energy gap ever exists, it must be smaller than the present spectroscopic resolution.

A related theoretical proposal concerns permanent exciton condensation in double-layer graphene [245, 246]. The idea is to separately contact the two layers, which are spaced by a dielectric medium, in order to induce the same quantity of charge with opposite sign in the two layers. With respect to the double-layer made of usual semiconductors mentioned in Section 19.2.3, here the advantage is the smaller value of the transverse electric field required to polarize the bilayer, due to the zero energy gap of graphene. The estimate of the Kosterlitz–Thouless temperature required to undergo the EI phase is debated theoretically [247–257]; recent Coulomb drag measurements [258, 259] point to the importance of inter-layer interactions.

In the absence of a dielectric spacer, undoped bilayer graphene is predicted—among other proposals—to undergo an excitonic ferroelectric phase that spontaneously breaks which-layer symmetry and polarizes the layers in charge [260–262]. The excitonic instability, which opens an energy gap, appears to sensitively depend on the interaction range [263]: in the case of finite range, the expected electronic phase is nematic and gapless [264, 265] (see reviews [266, 267]). The experimental observation of a transport gap at the charge neutrality point is controversial [268–271].

Other interesting graphene-based systems are carbon nanotubes, which may be thought of as wrapped sheets of graphene [272]. Since nanotube electronic states are built from those of graphene after imposing suitable boundary conditions,they exhibit perfect electron-hole symmetry [273] and hence provide the optimal nesting of energy bands to achieve permanent exciton condensation. Besides, Coulomb interactions are especially strong due to the reduced dimensionality of the system. Solving the effective-mass Bethe–Salpeter equation for spinless excitons, Ando [274] (and later Hartmann and coworkers [275]) found that electron–hole Coulomb attraction is below the critical threshold for the transition to the excitonic insulator. Later, Rontani [276] suggested that inter-valley exchange interaction affecting triplet excitons may lead to an excitonic instability. This instability does not depend on the size of the energy gap, which is modulated by the axial magnetic field, as a consequence of the relativistic nature of Dirac fermions. Moreover, the excitonic ground state increases the quasiparticle magnetization, which could shed some light on recent experiments in ultraclean devices [277].

19.3 Two-band versus BCS model

In this section we contrast the mean-field theory of the EI to the BCS theory of superconductors. We compare the equations of two model junctions, (i) one between EI and semimetal (SM–EI), (ii) the other one between superconductor

and normal metal (N–S). In both cases the phase boundary is due to the variation of the order parameter that changes along the direction perpendicular to the interface, tending respectively to zero in the bulk normal phase and to a constant value inside the condensed phase. The quasiparticle amplitudes for both SM–EI and N–S junctions are formally identical and are used in Section 19.4 to compute the flow of charge and heat through the junction.

19.3.1 The SM–EI junction

We start studying the junction between semimetal (SM) and EI on the basis of a spinless two-band model. The SM has overlapping isotropic conduction and valence bands (b and a, respectively) of opposite curvature and one electron per unit cell, hence the Fermi surface is a sphere in momentum space, located at the nesting of the two bands; since there are N electrons and $2N$ states available, the nesting occurs at zero energy in Fig. 19.1. One may turn the SM into an EI by either changing the SM stoichiometric composition through suitable alloying or applying stress, which opens a gap of size 2Δ in the bulk EI in virtue of the strong inter-band Coulomb interaction [cf. right panel of Fig. 19.1(a)]. The variation of the EI order parameter $\Delta(\boldsymbol{r})$ (defined below) along the coordinate z normal to the interface determines the effective interface potential, as shown in Fig. 19.2(a).

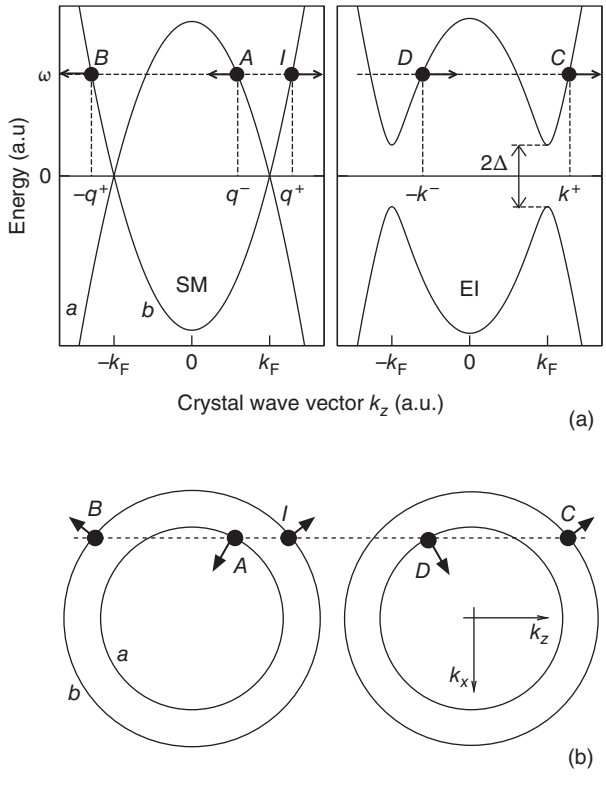

Fig. 19.1 Junction between semimetal (SM, left) and excitonic insulator (EI, right). (a) Quasiparticle energy ω vs wavevector k_z. The labels mark the allowed elastic scattering channels for an incoming electron (labeled I) with $k_z = q^+$. In particular, A is the interband (Andreev) reflection, B the intraband reflection, C the intraband transmission, and D the interband transmission. The size of the EI gap is 2Δ. (b) Isoenergetic contour lines in the (k_x, k_z) space for the energy ω shown in panel a. The arrows point to the group velocities of electrons in the different scattering channels.

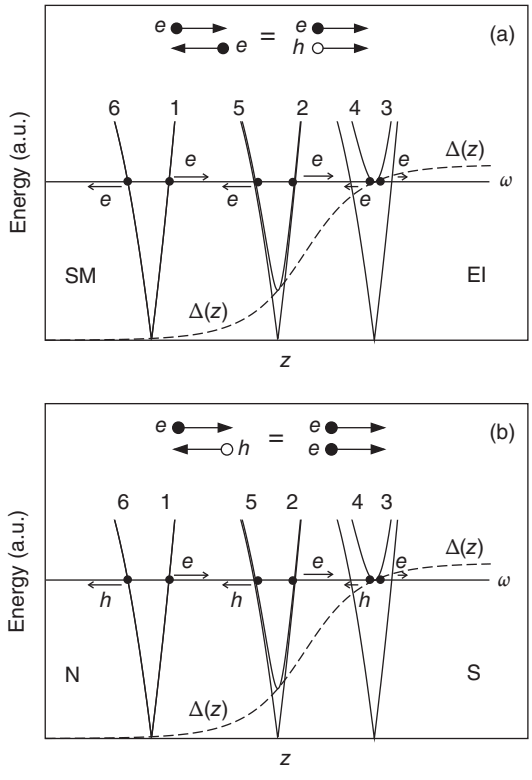

Fig. 19.2 Andreev reflection. (a) SM–EI junction. An incoming *b*-band electron is backscattered into the *a* band. The thicker (thinner) curves are the renormalized (bare) bands at different values of the z coordinate, with $\Delta(z)$ being the corresponding order parameter. Only the relevant low-energy portion of the spectrum is shown here, with numbers from 1 to 6 pointing to the time sequence of the reflection process (the arrows represent group velocities). The inset illustrates that the reflection process may alternatively be seen as a coherent flow of excitons from the SM into the EI. (b) N–S junction. In contrast to panel (a) an electron is backscattered as a hole, hence the whole process may be thought of as the dissipationless flow of Cooper pairs through the interface.

The hamiltonian of the SM–EI junction is

$$\mathcal{H}_{\text{SM–EI}} = \mathcal{H}_0 + \mathcal{H}_1 + \mathcal{H}_2. \tag{19.1}$$

Here $\mathcal{H}_1$ is the kinetic term which embodies the effect of the ideal and frozen crystal lattice on electrons with the envelope function in the effective mass approximation [278]:

$$\mathcal{H}_1 = \sum_{i=a,b} \int \mathrm{d}\boldsymbol{r}\, \psi_i^\dagger(\boldsymbol{r})\, \varepsilon_i(\boldsymbol{r})\, \psi_i(\boldsymbol{r})\,. \tag{19.2}$$

The field operator $\psi_a(\boldsymbol{r})$ [$\psi_b(\boldsymbol{r})$] annihilates an electron in the valence (conduction) energy band at the position $\boldsymbol{r}$ in space. The real-space band operators $\varepsilon_i(\boldsymbol{r})$ appearing in Eq. (19.2) take the form:

$$\varepsilon_a(\boldsymbol{r}) = G/2 + (2m)^{-1}\nabla^2; \tag{19.3a}$$

$$\varepsilon_b(\boldsymbol{r}) = -\,G/2 - (2m)^{-1}\nabla^2. \tag{19.3b}$$

Here m is the (positive) effective mass, G is the (positive) band overlap, and the energies are measured from the Fermi surface [45]. Throughout this work we put $\hbar = 1$ and assume that the system has unit volume. The valence- and conduction-band energy levels of the non-interacting bulk crystal, eigenvalues of $\mathcal{H}_1$, are

$$\varepsilon_a(\boldsymbol{k}_a) = G/2 - (2m)^{-1}k_a^2, \tag{19.4a}$$

$$\varepsilon_b(\boldsymbol{k}_b) = -G/2 + (2m)^{-1}k_b^2, \tag{19.4b}$$

where $\boldsymbol{k}_a$ and $\boldsymbol{k}_b$ refer to the respective band extrema. We assume the valence-band has a single maximum at $\boldsymbol{k} = 0$ whereas the conduction-band a single minimum at $\boldsymbol{k} = \boldsymbol{w}$, and ignore complications due to the presence of equivalent extrema. The Fermi wavevector is given by $k_{\rm F}^2 = mG$. The two-body term $\mathcal{H}_2$ consists of the inter-band Coulomb interaction,

$$\mathcal{H}_2 = \int \mathrm{d}\boldsymbol{r}\,\mathrm{d}\boldsymbol{r}'\,\psi_a^\dagger(\boldsymbol{r})\,\psi_b^\dagger(\boldsymbol{r}')\,V_2(\boldsymbol{r}-\boldsymbol{r}')\,\psi_b(\boldsymbol{r}')\,\psi_a(\boldsymbol{r})\,, \tag{19.5}$$

with $V_2(\boldsymbol{r})$ being the dielectrically screened Coulomb potential [43]. Renormalization effects due to intra-band Coulomb interaction and temperature dependence are taken into account into the energy band structure (19.4). The one-body term $\mathcal{H}_0$ is the sum of two parts,

$$\mathcal{H}_0 = \mathcal{V} + \mathcal{V}_{\rm hyb}. \tag{19.6}$$

$\mathcal{V}$ is the intra-band term,

$$\mathcal{V} = \sum_{i=a,b}\int \mathrm{d}\boldsymbol{r}\,\psi_i^\dagger(\boldsymbol{r})\,V(\boldsymbol{r})\,\psi_i(\boldsymbol{r})\,, \tag{19.7}$$

which includes the effects of the band offset as well as those of possible impurities and defects at the interface, such as a thin insulating layer, via the single-particle potential $V(\boldsymbol{r})$. The potential $V(\boldsymbol{r})$ can also include the effect of a voltage bias applied to the junction in a steady-state regime. The inter-band term,

$$\mathcal{V}_{\rm hyb} = \int \mathrm{d}\boldsymbol{r}\,\psi_b^\dagger(\boldsymbol{r})\,V_{\rm hyb}(\boldsymbol{r})\,\psi_a(\boldsymbol{r}) + \text{H.c.}, \tag{19.8}$$

hybridizes b and a bands by means of the potential $V_{\rm hyb}(\boldsymbol{r})$. This term may be originated e.g., by the change of an element in the SM compound. The influence of the potential $V_{\rm hyb}(\boldsymbol{r})$ on exciton condensation, which depends on the symmetry of the bands involved, is discussed in [178, 181, 185].

Both the hybridization potential and the EI order parameter contribute additively to the small band gap formed between the two overlapping bands [cf. right panel in Fig. 19.1(a)] hence their separate contributions cannot be distinguished by spectroscopy, as it was early recognized [45, 62, 279]. However, in this chapter we show that the transport properties across the SM–EI junction are distinctive features of the EI. The key point is in the length scale of the variation of the effective interface potential which reflects or transmits the electron. A component of the effective potential is the position dependent order parameter $\Delta(\mathbf{r})$, which decreases from the bulk value in the EI region to zero in the SM region [see Fig. 19.2(a)]. The length scale of the change is the coherence length in the EI, much longer than the lattice constant. Since this scenario is most likely if the lattices of the two components are as similar as possible, we classify as homogeneous the junction with $\Delta(\mathbf{r})$ being the only contribution to the interface potential.

On the other hand, the one-electron interface potential $V_{\rm hyb}(\boldsymbol{r})$ due to the change in hybridization has an abrupt variation on a length scale of the order of a few atomic layers, thus considered in our context as a heterogeneous junction (this includes the case of a Schottky barrier). We have studied the common physical features of the heterogeneous junction, including the abrupt band edge discontinuity, the short-ranged interface potential, and the impurities at the interface. Whereas the charge carriers in the heterogeneous junction experience uninteresting intraband reflection, electrons in the homogeneous junction change valley when backscattered as a feature of the EI band mixing. In the rest of the chapter we focus on the homogeneous junction and refer the reader elsewhere [59] for the study of the heterogeneous junction (corresponding to the case $V_{\rm hyb}(\boldsymbol{r}) \neq 0$).

Following Sham and Rice [6], we introduce the electron quasiparticle amplitudes,

$$f(\boldsymbol{r},t) = \langle\Psi_0|\tilde{\psi}_b(\boldsymbol{r},t)|\Psi^e_{\boldsymbol{k}}\rangle, \tag{19.9a}$$

$$g(\boldsymbol{r},t) = \langle\Psi_0|\tilde{\psi}_a(\boldsymbol{r},t)|\Psi^e_{\boldsymbol{k}}\rangle. \tag{19.9b}$$

Here $|\Psi_0\rangle$ and $|\Psi^e_{\boldsymbol{k}}\rangle$ are the exact interacting ground states with N and $N+1$ electrons, respectively; the quantum index $\boldsymbol{k}$ labeling the electron quasiparticle means the crystal momentum only in the bulk phase as the overall translational symmetry is destroyed by the presence of the junction. States and operators are written in the Heisenberg representation [280] (flagged by the tilde symbol on operators):

$$\tilde{\psi}_i(\boldsymbol{r},t) = \exp(\mathrm{i}\,[\mathcal{H}-\mu\,\mathcal{N}]\,t)\;\psi_i(\boldsymbol{r})\exp(-\mathrm{i}\,[\mathcal{H}-\mu\,\mathcal{N}]\,t), \tag{19.10}$$

where μ is the chemical potential (here $\mu = 0$ due to electron–hole symmetry) and the number operator $\mathcal{N}$ is defined by

$$\mathcal{N} = \sum_{i=a,b}\int \mathrm{d}\boldsymbol{r}\;\psi^\dagger_i(\boldsymbol{r})\;\psi_i(\boldsymbol{r}). \tag{19.11}$$

Writing down the Heisenberg equations of motion for the operators $\tilde{\psi}_i(\boldsymbol{r},t)$, exploiting the mean-field approximation to express them in a closed form, and neglecting unessential intra-band Hartree terms, we derive a set of two coupled integro-differential equations for the amplitudes $f(\boldsymbol{r},t)$ and $g(\boldsymbol{r},t)$:

$$\mathrm{i}\frac{\partial f(\boldsymbol{r},t)}{\partial t} = \left[-\frac{\nabla^2}{2m} - \frac{k_{\rm F}^2}{2m} + V(\boldsymbol{r})\right] f(\boldsymbol{r},t) + \int \mathrm{d}\boldsymbol{r}'\,\Delta\left(\boldsymbol{r},\boldsymbol{r}'\right)\,g\left(\boldsymbol{r}',t\right), \tag{19.12a}$$

$$\mathrm{i}\frac{\partial g(\boldsymbol{r},t)}{\partial t} = \left[\frac{\nabla^2}{2m} + \frac{k_{\rm F}^2}{2m} + V(\boldsymbol{r})\right] g(\boldsymbol{r},t) + \int \mathrm{d}\boldsymbol{r}'\,\Delta^*\left(\boldsymbol{r}',\boldsymbol{r}\right) f\left(\boldsymbol{r}',t\right). \tag{19.12b}$$

The built-in coherence of the exciton condensate, $\Delta\left(\boldsymbol{r},\boldsymbol{r}'\right)$, appearing in Eqs. (19.12) for $k > k_{\rm F}$ is defined as

$$\Delta\left(\boldsymbol{r},\boldsymbol{r}'\right) = V_2\left(\boldsymbol{r}-\boldsymbol{r}'\right)\,\langle\Psi_0|\tilde{\psi}_b(\boldsymbol{r})\,\tilde{\psi}^\dagger_a\left(\boldsymbol{r}'\right)|\Psi_0\rangle. \tag{19.13}$$

Except for the factor $V_2(\boldsymbol{r}-\boldsymbol{r}')$, $\Delta(\boldsymbol{r},\boldsymbol{r}')$ is the exciton macroscopic wave function. In fact, $\langle\Psi_0|\tilde{\psi}_b(\boldsymbol{r})\,\tilde{\psi}_a^\dagger(\boldsymbol{r}')\,|\Psi_0\rangle$ is the average on the many-electron ground state of the operator destroying an electron–hole pair, i.e., one b-band electron at $\boldsymbol{r}$ and one a-band hole at $\boldsymbol{r}'$ [the electron creation operator $\tilde{\psi}_a^\dagger(\boldsymbol{r}')$ may be regarded as a hole destruction operator]. Such average is zero in the SM phase, since for $k > k_\mathrm{F}$ b-band levels are empty and a-band levels filled, but it acquires a finite value in the EI phase. Besides, the finiteness of $\Delta(\boldsymbol{r},\boldsymbol{r}')$ reflects the new periodicity in real space of the EI phase, as the electron density shows an additional charge-density-wave-like order characterized by the wavevector $\boldsymbol{w}$ displacing the extrema of a and b bands [48]. For $k < k_\mathrm{F}$ the roles of electrons and holes are exchanged hence the definition (19.13) of $\Delta(\boldsymbol{r},\boldsymbol{r}')$ is modified accordingly.

The built-in coherence $\Delta(\boldsymbol{r},\boldsymbol{r}')$ generically depends on both center-of-mass and relative-motion coordinates, but inside the EI bulk the center-of-mass part of the condensate wave function is a plane wave with zero momentum, hence Δ depends only on the relative coordinate $\boldsymbol{r}-\boldsymbol{r}'$. We expect $\Delta(\boldsymbol{r}-\boldsymbol{r}')$ to smoothly vanish when $|\boldsymbol{r}-\boldsymbol{r}'|$ becomes larger than the characteristic length, the exciton radius. This allows us to easily find the bulk solution of the system of Eqs. (19.12) [$V(\boldsymbol{r}) = 0$] in terms of the two-component plane wave

$$\begin{pmatrix} f_{\boldsymbol{k}}(\boldsymbol{r},t) \\ g_{\boldsymbol{k}}(\boldsymbol{r},t) \end{pmatrix} = \begin{pmatrix} u_{\boldsymbol{k}} \\ v_{\boldsymbol{k}} \end{pmatrix} \mathrm{e}^{\mathrm{i}(\boldsymbol{k}\cdot\boldsymbol{r}-\omega t)}, \tag{19.14}$$

with energy

$$\omega(\boldsymbol{k}) = \sqrt{\xi_{\boldsymbol{k}}^2 + |\Delta_{\boldsymbol{k}}|^2}, \tag{19.15}$$

where $\xi_{\boldsymbol{k}} = \left(k^2 - k_\mathrm{F}^2\right)/(2m)$ and $\Delta_{\boldsymbol{k}}$ is the Fourier component of $\Delta(\boldsymbol{r})$. The amplitudes are normalized as

$$|u_{\boldsymbol{k}}|^2 = \frac{1}{2}\left(1 + \frac{\xi_{\boldsymbol{k}}}{E_{\boldsymbol{k}}}\right), \qquad |u_{\boldsymbol{k}}|^2 + |v_{\boldsymbol{k}}|^2 = 1, \tag{19.16}$$

and the relative phase between $u_{\boldsymbol{k}}$ and $v_{\boldsymbol{k}}$ is given by

$$\frac{u_{\boldsymbol{k}}}{v_{\boldsymbol{k}}} = \frac{\Delta_{\boldsymbol{k}}}{\omega(\boldsymbol{k}) - \xi_{\boldsymbol{k}}}. \tag{19.17}$$

When $\Delta_{\boldsymbol{k}} = 0$, the amplitude (19.14) is the trivial solution with $u_{\boldsymbol{k}} = 1$ and $v_{\boldsymbol{k}} = 0$, i.e., a conduction-band plane wave. When excitons form a condensate, solution (19.14) is admissible only if the self-consistency condition derived by the definition of $\Delta(\boldsymbol{r})$ is satisfied. This condition, which can be easily obtained from Eq. (19.13), is formally analogous to the BCS gap equation:

$$\Delta_{\boldsymbol{k}} = \sum_{\boldsymbol{p}} \frac{V_{2,\boldsymbol{k}-\boldsymbol{p}}\,\Delta_{\boldsymbol{p}}}{2\omega(\boldsymbol{p})}, \tag{19.18}$$

with $V_{2,\boldsymbol{k}}$ being the Fourier component of $V_2(\boldsymbol{r})$.

In general, the amplitudes $f(\boldsymbol{r},t)$ and $g(\boldsymbol{r},t)$ are the position space representation of the stationary electron-like elementary excitation across the *whole* junction. Taken together, they signify the wave function of the quasiparticle:

$f(g)$ is the probability amplitude for an electron of belonging to the conduction (valence) band. They satisfy the normalization condition

$$\int \mathrm{d}\boldsymbol{r}\,\left[|f(\boldsymbol{r},t)|^2 + |g(\boldsymbol{r},t)|^2\right] = 1, \tag{19.19}$$

and have always positive excitation energy ω due to the definitions (19.9–19.10). The probability current density $\boldsymbol{J}(\boldsymbol{r},t)$ can be found starting from the definition of the probability density $\rho(\boldsymbol{r},t)$ for finding either a conduction- or a valence-band electron at a particular time and place, $\rho(\boldsymbol{r},t) = |f|^2 + |g|^2$. After some manipulation of the equations of motion (19.12), one derives the continuity equation

$$\frac{\partial \rho}{\partial t} + \nabla \cdot \boldsymbol{J} = 0, \tag{19.20}$$

where

$$\boldsymbol{J} = \mathrm{Im}\left\{f^* \frac{\nabla}{m} f - g^* \frac{\nabla}{m} g\right\}. \tag{19.21}$$

Note that the two terms appearing in the rhs of Eq. (19.21), referring respectively to conduction and valence band electrons, have opposite sign since the curvature of the two bands is opposite. One can verify that the semiclassical group velocity of the quasiparticle, $\boldsymbol{v}_\mathrm{g} = \nabla_{\boldsymbol{k}}\,\omega$, coincides with the velocity $\boldsymbol{v}$ given by the full quantum mechanical expression (19.21), with $\boldsymbol{J} = \rho\,\boldsymbol{v}$.

19.3.2 The N–S junction

In this section we highlight the suggestive parallelism between the formalism introduced in Section 19.3.1 and the treatment of quasiparticle excitations in conventional superconductors, as modeled by the BCS theory.

The Hamiltonian of the N–S junction is

$$\mathcal{H}_{\mathrm{N\text{–}S}} = \mathcal{H}'_0 + \mathcal{H}'_1 + \mathcal{H}'_2. \tag{19.22}$$

Electrons in the metal experience the crystal lattice potential through $\mathcal{H}'_1$,

$$\mathcal{H}'_1 = -\frac{1}{2m} \sum_{\sigma=\uparrow,\downarrow} \int \mathrm{d}\boldsymbol{r}\,\psi^\dagger_\sigma(\boldsymbol{r})\,\nabla^2 \psi_\sigma(\boldsymbol{r})\,. \tag{19.23}$$

The space-dependent field operator $\psi_\sigma(\boldsymbol{r})$ annihilates an electron with spin σ in the twofold degenerate conduction energy band, whose energy dispersion is taken to be parabolic for simplicity,

$$\varepsilon(\boldsymbol{k}) = k^2/(2m), \tag{19.24}$$

$\varepsilon(\boldsymbol{k})$ being the eigenvalue of $\mathcal{H}'_1$. With respect to the SM, the role of a and b bands is replaced by the two spin flavors $\uparrow$ and $\downarrow$. The Fermi wavevector k_F is fixed by the condition that there are N electrons in the system, with $\mu = k_\mathrm{F}^2/2m$.

The relevant two-body interaction $\mathcal{H}'_2$ is attractive and short-ranged,

$$\mathcal{H}'_2 = -g \int \mathrm{d}\boldsymbol{r}\,\psi^\dagger_\uparrow(\boldsymbol{r})\,\psi^\dagger_\downarrow(\boldsymbol{r})\,\psi_\downarrow(\boldsymbol{r})\,\psi_\uparrow(\boldsymbol{r})\,, \tag{19.25}$$

with g being a positive constant parametrizing the combined effect of Coulomb and electron–phonon interaction in the vicinity of the Fermi surface [56]. The short-range interaction (19.25) does not affect electrons with parallel spin as a consequence of Pauli exclusion principle. The effective potential (19.25) results from the competition between Coulomb repulsion and the screening effect of the positive ions in the lattice. Close to the resonance frequency of the ion motion, the ions give a very large response to the perturbation induced by an electron charge. The resulting cloud of the moving electron plus the polarized ions has a net positive charge, then inducing a weak electron-electron attraction, whose characteristic energy is a tiny fraction of the Fermi energy. As in the case of the SM–EI junction, the boundary between N and S phases is determined by the variation along z of the pair potential associated to $\mathcal{H}_2'$, defined below [see Fig. 19.2(b)]. A residual effect of Coulomb interaction is to shift the energy levels, that are already renormalized in the dispersion relation (19.24). The one-body term

$$\mathcal{H}_0' = \sum_{\sigma=\uparrow,\downarrow} \int \mathrm{d}\boldsymbol{r}\, \psi_\sigma^\dagger(\boldsymbol{r})\, V'(\boldsymbol{r})\, \psi_\sigma(\boldsymbol{r}), \tag{19.26}$$

arises from the possible impurities and defects at the interface, as well as the applied bias voltage.

In order to find out the quasiparticles of the N–S junction, we follow the same approach as for the SM–EI junction, with one important difference [281] that derives from the following definition of the amplitudes:

$$f'(\boldsymbol{r},t) = \langle \Psi_0' | \tilde{\psi}_\uparrow(\boldsymbol{r},t) | \Psi_{\boldsymbol{k}}^b \rangle, \tag{19.27a}$$

$$g'(\boldsymbol{r},t) = \langle \Psi_0' | \tilde{\psi}_\downarrow^\dagger(\boldsymbol{r},t) | \Psi_{\boldsymbol{k}}^b \rangle. \tag{19.27b}$$

Here $|\Psi_{\boldsymbol{k}}^b\rangle$ is the state with one quasiparticle added to the many-electron ground state $|\Psi_0'\rangle$. According to Eqs. (19.27), the number of particles is not a constant of motion, as we add both an electron [Eq. (19.27a)] and a hole [Eq. (19.27b)] to $|\Psi_0'\rangle$. This is allowed within the grand canonical framework, where the chemical potential μ is the independent thermodynamic variable instead of N.

The resulting 'Bogoliubov–de Gennes' equations of motion are:

$$\mathrm{i}\frac{\partial f'(\boldsymbol{r},t)}{\partial t} = \left[-\frac{\nabla^2}{2m} - \frac{k_\mathrm{F}^2}{2m} + V'(\boldsymbol{r})\right] f'(\boldsymbol{r},t) + \Delta'(\boldsymbol{r})\, g'(\boldsymbol{r},t), \tag{19.28a}$$

$$\mathrm{i}\frac{\partial g'(\boldsymbol{r},t)}{\partial t} = \left[\frac{\nabla^2}{2m} + \frac{k_\mathrm{F}^2}{2m} - V'(\boldsymbol{r})\right] g'(\boldsymbol{r},t) + \Delta'^*(\boldsymbol{r}) f'(\boldsymbol{r},t), \tag{19.28b}$$

with the local pair potential $\Delta'(\boldsymbol{r})$ being defined as

$$\Delta'(\boldsymbol{r}) = -g \langle \Psi_0' | \tilde{\psi}_\downarrow(\boldsymbol{r})\, \tilde{\psi}_\uparrow(\boldsymbol{r}) \, | \Psi_0' \rangle. \tag{19.29}$$

The space-dependent parameter $\Delta'(\boldsymbol{r})$ may be regarded as the center-of-mass wave function of the condensate made of Cooper pairs. The latter are bound pairs of two electrons with opposite spins, as it is evident from the definition (19.29). The product of the two operators that destroys a Cooper pair, appearing in the so-called anomalous average (19.29), does not commute with the

number operator $\mathcal{N}$ as it breaks the $U(1)$ gauge symmetry of total hamiltonian $\mathcal{H}_{\text{N–S}}$. Nevertheless, since the number of electrons is macroscopic, the number fluctuations, of order $\sqrt{N}$, are small and may be neglected with respect to the average value of N. Moreover, since a value of one or two is still small with respect to $\sqrt{N}$, the ground states with either N or $N-2$ electrons must be regarded as identical, so the anomalous character (i.e., breaking the gauge symmetry of $\mathcal{H}_{\text{N–S}}$) of the definitions (19.29) and (19.27) is physically irrelevant.

It is remarkable to observe that the systems of equations, (19.12) and (19.28), respectively, describing the SM–EI and the N–S junctions, are formally identical in the homogeneous case. This corresponds to put respectively $V(\boldsymbol{r}) = 0$ in Eqs. (19.12) and $V'(\boldsymbol{r}) = 0$ in Eqs. (19.28), as well as to take the built-in exciton coherence in Eq. (19.12) as a local operator, $\Delta\left(\boldsymbol{r}, \boldsymbol{r}'\right) = \delta\left(\boldsymbol{r} - \boldsymbol{r}'\right) \Delta(\boldsymbol{r})$ (then $\Delta_{\boldsymbol{k}}$ does not depend on $\boldsymbol{k}$). However, the quasiparticle amplitudes for the two model junctions signify profoundly different types of single-particle excitations.

In the EI, to obtain a free electron in the b-band—for $k > k_{\text{F}}$—one has to break an exciton among those forming the condensate, that is a bound pair of a b-band electron and a-band hole. The way to do this is to either create an electron in the b band, whose amplitude component is f, or destroy a hole in the a band, whose amplitude component is g.

In the S, to obtain an unbounded single particle with spin $\uparrow$, one has to break a Cooper pair in the condensate. This is accomplished by means of either creating an electron with spin $\uparrow$ or destroying an electron with spin $\downarrow$. The latter option is equivalent to creating a hole with spin $\uparrow$, as a consequence of time-reversal symmetry. The components f' and g' are the amplitudes for the propagation of the electron and the hole, respectively. Table 19.1 compares the key features of the EI with those of the S, with regard to both the ground state and the quasiparticle excitations.

In the following we are interested in comparing the SM–EI and N–S systems. In order to stress their formal analogy, hereafter we drop the prime symbol to label quantities referring to the N–S junction (as f, g, Δ, etc.) and use the same notation in both cases. With this convention, formulae (19.14–19.21) obtained for the SM–EI junction hold for the N–S junction, too.

19.4 Andreev reflection at the interface between excitonic insulator and semimetal

In this section we introduce the phenomenon of Andreev reflection at the N–S boundary as a paradigm to discuss the transport through the SM–EI junction. There are three qualitatively important results that are common to both systems: (i) all three Cartesian components of the velocity change sign when the quasiparticle is reflected (Section 19.4.1) (ii) the ratio of incident quasiparticles $C(\omega)$ which are transmitted through the interface depends on the coherence factors of the condensate, being strongly suppressed close to the gap (Section 19.4.2) (iii) the condensate induces pairing on the normal side of the junction (proximity effect, Section 19.4.3).

19.4.1 Velocity inversion at the interface

The electrical transport across the N–S junction exhibits high conductance behavior at vanishing applied voltage bias. This evidence seems to contradict the fact that quasiparticle excitations are gapped in the S (see Fig. 19.3): quasiparticles in the bulk N approaching the junction with energy smaller than the gap, $0 < \omega < \Delta$, cannot penetrate into the bulk S. This paradox is solved by Andreev reflection, which is illustrated below.

Consider $\Delta(z)$ to be a smooth complex increasing function of z, tending respectively to the asymptotic values zero when $z \to -\infty$, inside the bulk N, and Δ_0 when $z \to +\infty$, inside the bulk S [Fig. 19.2(b)]. Following Andreev [281], we note that the medium under consideration is completely homogeneous with an accuracy $2m|\Delta_0|/k_F^2$—a very small quantity in typical superconductors. Therefore, we seek a solution of Eqs. (19.28) in the form

$$f(\boldsymbol{r}) = \mathrm{e}^{\mathrm{i}k_F \boldsymbol{n}\cdot\boldsymbol{r}}\eta(\boldsymbol{r}), \qquad g(\boldsymbol{r}) = \mathrm{e}^{\mathrm{i}k_F \boldsymbol{n}\cdot\boldsymbol{r}}\chi(\boldsymbol{r}), \tag{19.30}$$

where $\boldsymbol{n}$ is some unit vector and $\eta(\boldsymbol{r})$ and $\chi(\boldsymbol{r})$ are functions that vary slowly compared to $\mathrm{e}^{\mathrm{i}k_F \boldsymbol{n}\cdot\boldsymbol{r}}$. Substituting Eq. (19.30) in Eq. (19.28) and neglecting higher derivatives of η and χ, we obtain

$$(\mathrm{i}v_F \boldsymbol{n}\cdot\nabla + \omega)\,\eta(\boldsymbol{r}) - \Delta(z)\,\chi(\boldsymbol{r}) = 0, \tag{19.31a}$$

$$(\mathrm{i}v_F \boldsymbol{n}\cdot\nabla - \omega)\,\chi(\boldsymbol{r}) + \Delta^*(z)\,\eta(\boldsymbol{r}) = 0, \tag{19.31b}$$

where $v_F = k_F/m$. It is easy to find for $z \to \pm\infty$ the asymptotic form of the solutions of Eqs. (19.31) describing the reflection of the quasiparticle falling on the junction. When $z \to -\infty$ we put $\Delta(z) = 0$. Then

$$\begin{pmatrix}\eta\\ \chi\end{pmatrix} = C_1\begin{pmatrix}1\\ 0\end{pmatrix}\mathrm{e}^{\mathrm{i}\boldsymbol{k}_1\cdot\boldsymbol{r}} + C_2\begin{pmatrix}0\\ 1\end{pmatrix}\mathrm{e}^{\mathrm{i}\boldsymbol{k}_2\cdot\boldsymbol{r}}, \tag{19.32}$$

where $\boldsymbol{n}\cdot\boldsymbol{k}_1 = \omega/v_F$, $\boldsymbol{n}\cdot\boldsymbol{k}_2 = -\omega/v_F$; C_1 and C_2 are arbitrary constants. The first term on the rhs of Eq. (19.32) corresponds to an electron whose velocity

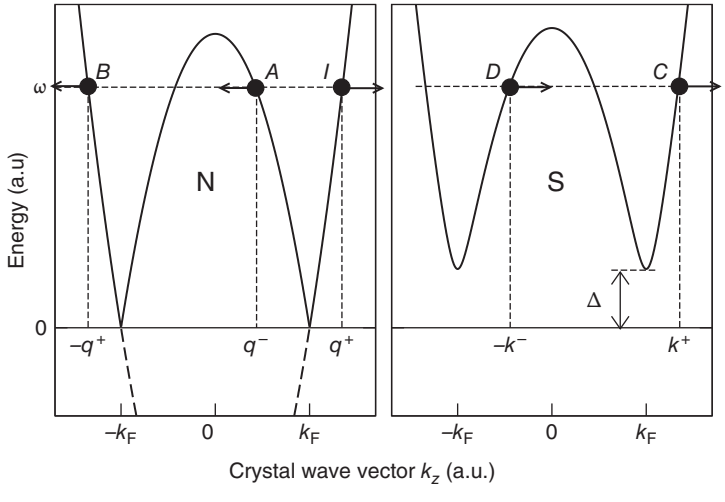

Fig. 19.3 Junction between normal metal (N, left) and superconductor (S, right). The plot shows the quasiparticle energy ω vs wavevector k_z in the two bulk phases. The labels mark the allowed elastic scattering channels for an incoming particle (labeled *I*) with $k_z = q^+$. *A* is the Andreev reflection, *B* the normal reflection, *C* the normal transmission, and *D* the cross-branch transmission. Note that the energy of the particle is positive: on the N side the hole branch for $|k_z| < k_F$ is obtained by inverting the energy of the portion of band filled with electrons (showed as a dashed curve) with respect to the Fermi surface.

$\boldsymbol{v}$ (or $\boldsymbol{J}$) lies along $\boldsymbol{n}$, and the second term to a hole whose velocity lies in the opposite direction to $\boldsymbol{n}$ (in fact $\omega/v_{\rm F} \ll k_{\rm F}$ since $2m\,|\Delta_0|\,/k_{\rm F}^2 \ll 1$). If $n_z > 0$, then the wave function (19.32) describes an electron incident on the boundary and reflected as a hole on the N side; if $n_z < 0$, it describes an incident hole reflected as an electron. When $z \to +\infty$ we put $\Delta(z) = \Delta_0$ in Eq. (19.31). The solution describing the transmitted wave ($J_z > 0$) has for $\omega > |\Delta_0|$ the form

$$\begin{pmatrix}\eta\\ \chi\end{pmatrix} = \frac{C_3}{\sqrt{2}}\begin{pmatrix}\sqrt{1+v_{\rm F}\boldsymbol{n}\cdot\boldsymbol{k}_3/\omega}\,{\rm e}^{{\rm i}\varphi/2}\\ \sqrt{1-v_{\rm F}\boldsymbol{n}\cdot\boldsymbol{k}_3/\omega}\,{\rm e}^{-{\rm i}\varphi/2}\end{pmatrix}{\rm e}^{{\rm i}\boldsymbol{k}_3\cdot\boldsymbol{r}}, \tag{19.33}$$

where C_3 is a constant, φ is the phase of Δ_0,

$$\boldsymbol{n}\cdot\boldsymbol{k}_3 = v_{\rm F}^{-1}\sqrt{\omega^2-|\Delta_0|^2} \quad \text{for} \quad n_z > 0, \tag{19.34a}$$

$$\boldsymbol{n}\cdot\boldsymbol{k}_3 = -v_{\rm F}^{-1}\sqrt{\omega^2-|\Delta_0|^2} \quad \text{for} \quad n_z < 0. \tag{19.34b}$$

As expected, for $\omega < |\Delta_0|$ the functions η and χ decay exponentially as $z \to +\infty$, hence the quasiparticle is prevented from entering the bulk S. However, all three Cartesian components of the velocity of the reflected particle change sign [see Fig. 19.4(b)]. This remarkable behavior, which is not due to interface roughness since we take the interface to be completely flat, is the key to explain the electric transport through the N–S junction. An electron with velocity $\boldsymbol{v}$ is Andreev-reflected into a hole with velocity $-\boldsymbol{v}$ which carries exactly the same current as the incident electron. In fact, in virtue of time-reversal invariance, the hole moving with velocity $-\boldsymbol{v}$ may be regarded as an electron moving with velocity $\boldsymbol{v}$ [Fig. 19.4(b)]. Therefore, we may understand the process of Andreev reflection as an electron above the Fermi surface forming a Cooper pair with another electron below the Fermi surface on the N side: such pair moves to the S side merging into the condensate, whereas the second electron leaves a hole behind in the N Fermi sea [282].

The results obtained in this section hold also for the SM–EI junction, provided one links η and χ components to the probability amplitudes of an electron of being in either b or a band, respectively, as illustrated in Fig. 19.4(a). Apparently, the reflection process at the SM–EI junction seems the usual reflection of an electron from the gap barrier. However, the complete reversal of the velocity vector suggests that the reflected electron may be regarded as an incoming hole with the same velocity as the incoming electron. The idea is that the overall reflection process may be thought of as the flow of electron–hole pairs—excitons—from the SM to the EI side, where they merge into the exciton condensate. Below we substantiate this alternate interpretation.

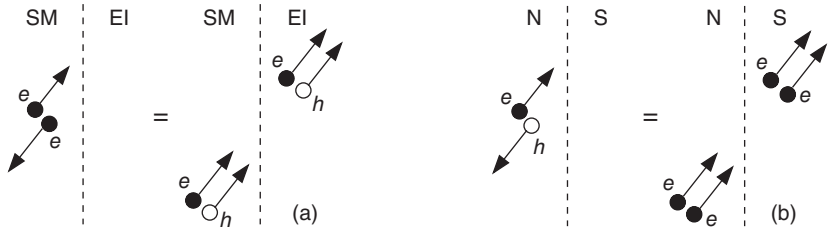

Fig. 19.4 Sketch of Andreev reflection for quasiparticles approaching the junction from the normal-phase side. (a) SM–EI junction. The reflected left-going electron is equivalent to a right-going hole. (b) N–S junction. The reflected left-going hole is equivalent to a right-going electron.

19.4.2 Coherence factors in the transmission coefficients

To proceed we specify the functional form of the interface potential, assuming that the excitonic coherence is a step function at the SM–EI interface, $\Delta(\boldsymbol{r}) = \Delta\,\theta(z)$, with $\Delta > 0$. Moreover, we introduce a simple-minded model for the effect of disorder at the origin (e.g., an insulating layer) through the δ-potential $V(\boldsymbol{r}) = H\,\delta(z)$. In the following we abandon the slowly varying amplitude approximation and look for solutions of the full Eqs. (19.28), requiring a larger number of scattering channels than those used in Section 19.4.1.

Carriers coming from the bulk SM with energies slightly outside the EI gap have, say for the incident electron at I, two reflection channels, A and B, and two transmission channels at C and D (see Fig. 19.1). If the energy lies within the gap, only the two reflection channels are possible. Whereas the interface—by breaking the lattice translational symmetry—can in principle connect different parts of the Brillouin zone [283], here the relevant regions of the wavevector space are the two valleys near the gaps in the bulk EI for those states with the same component of the wavevector parallel to the interface.

We consider the elastic scattering at equilibrium, matching wave functions of the incident (I), transmitted (C and D), and reflected (A and B) states at the boundary, following the approach of [284]. In the bulk EI, there are a pair of magnitudes of k associated with ω, namely

$$k^{\pm} = \sqrt{2m}\sqrt{k_{\rm F}^2/2m \pm \left(\omega^2 - \Delta^2\right)^{1/2}}. \tag{19.35}$$

The total degeneracy of relevant states for each ω is fourfold: $\pm k^{\pm}$. The two states $\pm k^{+}$ have a dominant conduction-band character, whereas the two states $\pm k^{-}$ are mainly valence-band states. Using the notation

$$\Psi(z) = \begin{pmatrix} f(z) \\ g(z) \end{pmatrix} \tag{19.36}$$

the wave functions degenerate in ω are

$$\Psi_{\pm k^{+}} = \begin{pmatrix} u_0 \\ v_0 \end{pmatrix} \mathrm{e}^{\pm \mathrm{i} k^{+} z}, \qquad \Psi_{\pm k^{-}} = \begin{pmatrix} v_0 \\ u_0 \end{pmatrix} \mathrm{e}^{\pm \mathrm{i} k^{-} z}, \tag{19.37}$$

with the amplitudes u_0, v_0 defined as

$$u_0 = \sqrt{\frac{1}{2}\left[1 + \frac{(\omega^2 - \Delta^2)^{1/2}}{\omega}\right]}, \quad v_0 = \sqrt{\frac{1}{2}\left[1 - \frac{(\omega^2 - \Delta^2)^{1/2}}{\omega}\right]}, \tag{19.38}$$

possibly extended in the complex manifold. With regard to the SM bulk, $\Delta = 0$ and the two possible magnitudes of the momentum q reduce to $q^{\pm} = [2m(k_{\rm F}^2/2m \pm \omega)]^{1/2}$, with wave functions

$$\Psi_{\pm q^{+}} = \begin{pmatrix} 1 \\ 0 \end{pmatrix} \mathrm{e}^{\pm \mathrm{i} q^{+} z}, \qquad \Psi_{\pm q^{-}} = \begin{pmatrix} 0 \\ 1 \end{pmatrix} \mathrm{e}^{\pm \mathrm{i} q^{-} z}, \tag{19.39}$$

for conduction and valence bands, respectively. The appropriate boundary conditions are: (i) Continuity of Ψ at $z = 0$, so $\Psi_{\rm EI}(0) = \Psi_{\rm SM}(0) \equiv \Psi(0)$. (ii) $\left[f'_{\rm EI}(0) - f'_{\rm SM}(0)\right]/(2m) = Hf(0)$ and $\left[g'_{\rm EI}(0) - g'_{\rm SM}(0)\right]/(2m) = -Hg(0)$, the derivative boundary conditions appropriate for δ-functions. (iii) Incoming

(incident), reflected and transmitted wave directions are defined by their group velocities, i.e., an electron incident from the left is transmitted with $v > 0$ and reflected with $v < 0$.

If an electron incident on the interface from the SM with energy $\omega > \Delta$ has wavevector q^+, the four outgoing channels, with probabilities A, B, C, D, have respectively wavevectors q^-, $-q^+$, k^+, $-k^-$, as shown in Fig. 19.1. C is the probability of transmission through the interface with a wavevector on the same (i.e., forward) side of the Fermi surface as q^+ (i.e., $q^+ \to k^+$, not $-k^-$), whereas D gives the probability of transmission on the back side of the Fermi surface (i.e., $q^+ \to -k^-$). B is the probability of intra-branch reflection, whereas A is the probability of Andreev (cross-branch) reflection. The steady state solution of system (19.12) is

$$\Psi_{\rm SM}(z) = \Psi_{\rm inc}(z) + \Psi_{\rm refl}(z), \qquad \Psi_{\rm EI}(z) = \Psi_{\rm trans}(z),$$

where

$$\Psi_{\rm inc}(z) = \begin{pmatrix}1\\0\end{pmatrix} e^{iq^+z}, \quad \Psi_{\rm refl}(z) = a\begin{pmatrix}0\\1\end{pmatrix} e^{iq^-z} + b\begin{pmatrix}1\\0\end{pmatrix} e^{-iq^+z},$$
$$\Psi_{\rm trans}(z) = c\begin{pmatrix}u_0\\v_0\end{pmatrix} e^{ik^+z} + d\begin{pmatrix}v_0\\u_0\end{pmatrix} e^{-ik^-z}. \tag{19.40}$$

Applying the boundary conditions, we obtain a system of four linear equations in the four unknowns a, b, c, and d, which we solve at a fixed value for ω. We introduce the dimensionless barrier strength $Z = H/v_{\rm F}$, and approximate $k^+ = k^- = q^+ = q^- \approx k_{\rm F}$, on the basis that the ratio $2m\Delta/k_{\rm F}^2$ is small. The quantities A, B, C, D, are the ratios of the probability current densities of the specific transmission or reflection channels to the current of the incident particle, e.g., $A = |J_A/J_{\rm inc}|$, and so on. The conservation of probability requires that

$$A + B + C + D = 1. \tag{19.41}$$

This result is useful in simplifying expressions for energies below the gap, $\omega < \Delta$, where there can be no transmitted electrons, so that $C = D = 0$. Then, Eq. (19.41) reduces simply to $A = 1 - B$.

We find

$$\begin{aligned} a &= \frac{u_0 v_0}{\gamma}, \\ b &= \frac{\left(u_0^2 - v_0^2\right) Z^2 - iZ}{\gamma}, \\ c &= \frac{u_0\,(1 + iZ)}{\gamma}, \\ d &= -\frac{iv_0 Z}{\gamma}, \end{aligned} \tag{19.42}$$

$$\gamma = Z^2\left(v_0^2 - u_0^2\right) + (iZ + 1/2)\,2u_0^2.$$

The probability coefficients are actually the currents, measured in units of $v_{\rm F}$. For example, $A = |J_A|/v_{\rm F} = |a|^2$, and $D = |d|^2 / \left|v_0^2 - u_0^2\right|$. The expression

Table 19.2 Transmission and reflection coefficients for the SM–EI junction. A gives the probability of Andreev reflection (cross-branch), B of ordinary reflection, C of transmission without branch crossing, and D of cross-branch transmission. Here $\theta = \omega^2 + 4Z^2\omega^2 + (1+4Z^4)(\Delta^2-\omega^2) - 8Z^3\omega\left(\Delta^2-\omega^2\right)^{1/2}$, $\gamma = Z^2\left(v_0^2-u_0^2\right) + (\mathrm{i}Z+1/2)\,2u_0^2$, and $u_0^2 = 1-v_0^2 = 1/2\,[1+(\omega^2-\Delta^2)^{1/2}/\omega]$.

	A	B	C	D
No condensate	0	$\frac{Z^2}{1+Z^2}$	$\frac{1}{1+Z^2}$	0
General form				
$\omega < \Delta$	$\frac{\Delta^2}{\theta}$	$1-A$	0	0
$\omega > \Delta$	$\frac{u_0^2 v_0^2}{\lvert\gamma\rvert^2}$	$\frac{\left(u_0^2-v_0^2\right)^2 Z^4+Z^2}{\lvert\gamma\rvert^2}$	$\frac{u_0^2\left(u_0^2-v_0^2\right)\left(1+Z^2\right)}{\lvert\gamma\rvert^2}$	$\frac{v_0^2\left(u_0^2-v_0^2\right)Z^2}{\lvert\gamma\rvert^2}$
No barrier				
$\omega < \Delta$	1	0	0	0
$\omega > \Delta$	$\frac{v_0^2}{u_0^2}$	0	$\frac{u_0^2-v_0^2}{u_0^2}$	0
Strong barrier				
$\omega < \Delta$	$\frac{\Delta^2}{4Z^4(\Delta^2-\omega^2)}$	$1-A$	0	0
$\omega > \Delta$	$\frac{u_0^2 v_0^2}{Z^4(u_0^2-v_0^2)^2}$	$1-\frac{1}{Z^2(u_0^2-v_0^2)}$	$\frac{u_0^2}{Z^2(u_0^2-v_0^2)}$	$\frac{v_0^2}{Z^2(u_0^2-v_0^2)}$

for the energy dependences of A, B, C, and D can be conveniently written in terms of the so-called coherence factors u_0 and v_0. The results are given in Table 19.2. For convenience, in addition to the general results we also list the limiting forms of the results for zero barrier ($Z = 0$) and for a strong barrier [$Z^2(u_0^2 - v_0^2) \gg 1$], as well as for $\Delta = 0$ (the semimetal case).

In the absence of disorder ($Z = 0$), the dependence of the transmission coefficient $C(\omega)$ on energies close to the gap is

$$C(\omega) = 2\sqrt{2\,(\omega-\Delta)\,/\Delta} \qquad \omega \approx \Delta, \tag{19.43}$$

whereas below the gap the electron is totally Andreev-reflected and the transmission is zero. The ordinary reflection channel is completely suppressed ($B = 0$) as well as cross-branch transmission ($D = 0$). The situation is depicted in Fig. 19.5(a). Even above the gap, $\omega > \Delta$, there is a high probability for Andreev reflection, which strongly depends on ω. For energies close to the gap, $\omega \approx \Delta$, Andreev reflection is almost certain, $A \approx 1$. This is the cause for the low value of interface conductance. The effect is washed out by the opacity of the interface: as $|Z|$ increases [$Z = -1$ in Fig. 19.5(b)], the total reflection probability $A + B$ loses its dependence on ω, and the dominant reflection channel changes from the Andreev one (A) into the ordinary one (B).

The interface opacity Z is the handle to tune the effect of excitonic coherence on transport, as discussed in the next sections. Remarkably, the overall set of results of Table 19.2 is formally identical to the analogous quantities obtained for the N–S junction (e.g., compare with Table II of [284]), the only slight difference being the behavior for $Z \neq 0$. In fact, due to the different boundary conditions, the coefficients of the N–S junction are even functions of Z, whereas those of Table 19.2 do not have a definite parity with respect to the sign of Z for $\omega < \Delta$ (there is a mistake in the entry corresponding to the sub-gap strong-barrier case appearing in Table II of Ref. [284]). Nevertheless,

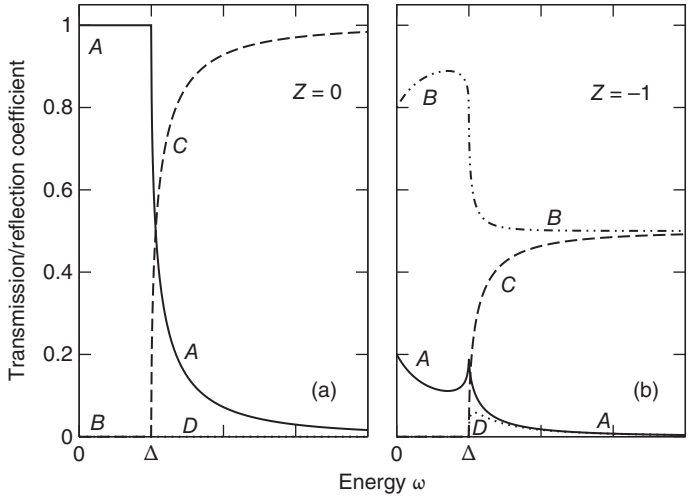

Fig. 19.5 Transmission and reflection coefficients at the SM–EI boundary vs. quasiparticle energy ω. (a) $Z = 0$. (b) $Z = -1$. A gives the probability of Andreev reflection, B gives the probability of ordinary reflection, C gives the transmission probability without branch crossing, and D gives the probability of transmission with branch crossing. The parameter Z measures the interface transparency.

the expressions for coefficients in the strong-barrier case are the same for the SM–EI and the N–S junction.

The appearance of coherence factors u and v in the coefficients of the SM–EI junction demonstrates that the electron–hole condensate strongly affects the transport and in general the wave function of carriers, by means of both inducing coherence on the SM side and altering transmission features.

19.4.3 Proximity effect

From the results of the previous two subsections it follows that the condensate on the right hand side of the junction induces pairing correlations in the normal phase on the left hand side, even if there the order parameter Δ is zero as interactions are switched off. In the N–S junction the pairing induced by the proximity effect correlates electrons with opposite spins, whereas in the SM–EI junction it correlates electron–hole pairs.

To show that the exciton condensate induces exciton order on the SM side it is sufficient to compute the built-in coherence $\langle\Psi_0|\tilde{\psi}_b(\boldsymbol{r})\,\tilde{\psi}_a^\dagger(\boldsymbol{r})|\Psi_0\rangle$. This would be zero in an isolated SM but by the proximity with the condensate acquires the value

$$\langle\Psi_0|\tilde{\psi}_b(\boldsymbol{r})\,\tilde{\psi}_a^\dagger(\boldsymbol{r})|\Psi_0\rangle = \sum_{\boldsymbol{k}} f_{\boldsymbol{k}}(\boldsymbol{r})\,g_{\boldsymbol{k}}^*(\boldsymbol{r})$$
$$\approx 2\int \mathrm{d}\,\omega\,N(\omega)\cos\left[\arctan\left(\frac{\Delta}{\omega}\right)+2\frac{\omega}{v_\mathrm{F}}z\right], \qquad (19.44)$$

with $N(\omega)$ being the density of states in the SM. Inside the gap ($\omega \approx 0$) each quasiparticle contributes to the sum (19.44) with a term $\sim \exp\left[\mathrm{i}\arctan(\Delta/\omega)+2\mathrm{i}\omega z/v_\mathrm{F}\right]$. The only coordinate dependence enters this expression via the phase factor, $2\omega z/v_\mathrm{F}$, which represents the relative phase shift of conduction- and valence-band components of the wave function. If $\omega = 0$, then these components keep constant relative phase $\arctan(\Delta/\omega)$ all the

way to $z = -\infty$, where no pairing interactions exist. Therefore, the reflected electron—equivalent to an incoming hole—has exactly the same velocity as the incident particle, and will thus retrace *exactly the same path* all the way to $z = -\infty$. At finite energy, the z dependent oscillations provide destructive interference on the pair coherence. Hence, the paths of incident and reflected electrons part ways away from the interface. Analogous considerations apply to the incident electron and to the Andreev-reflected hole in a sub-gap scattering event at the N–S interface [282].

19.5 A perfect insulator

From the results for transmission and reflection probabilities obtained in Section 19.4.2, we derive in the linear response regime the values of the electrical and thermal conductances of the SM–EI junction, G and G_T, respectively. The derivation is standard and it proceeds along the lines explained for example in [180, 284, 285]. The Seebeck coefficient is zero due to the symmetry of the model [180, 286]. Then, except for an additive phonon contribution to the thermal conductance, the interface thermoelectric properties are completely determined by G and G_T.

Both G and G_T have an activation threshold at low temperature, T, proportional to the gap Δ, as shown in Fig. 19.6 (cf. the curves for the transparent barrier with $Z = 0$). At first sight, the transport properties of the SM–EI junction seem dramatically different from those of the N–S junction, as the latter may sustain an electric supercurrent at vanishing bias voltage whereas the former exhibits insulating behavior. However, a closer examination shows that the two junctions share essential features.

In fact, the functional dependence of G_T on T and Δ is the same for both the SM–EI and N–S junctions. Remarkably, the time rate of entropy production, $\dot{S}$, is the same very low value in both cases, pointing to the disipationless character of the flow of charge and heat. This is seen by the relation between $\dot{S}$ and the transport coefficients [286],

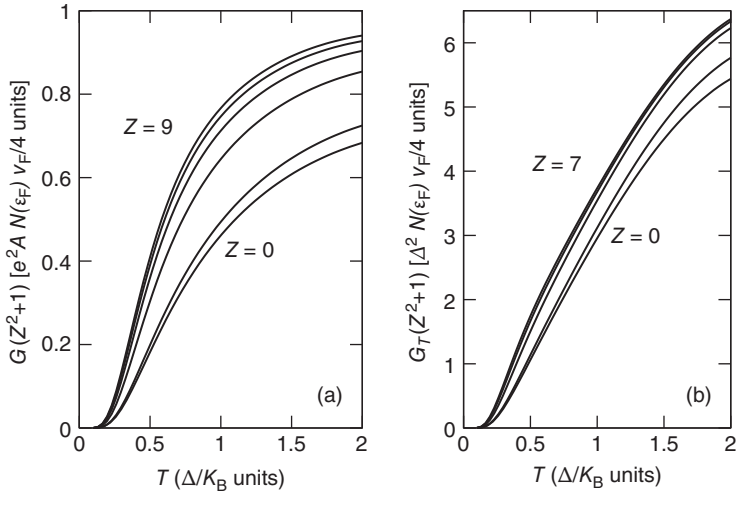

Fig. 19.6 (a) Electrical conductance G of the SM–EI junction vs temperature T. The curves correspond to different values of the dimensionless barrier opacity, $Z = 0, 1, 3, 5, 7, 9$. For each value of Z, G is divided by the corresponding transmission coefficient when $\Delta = 0$, i.e., $C_{\Delta=0} = (Z^2 + 1)^{-1}$. K_B is the Boltzmann constant, $\mathcal{A}$ is the interface cross-sectional area, $N(\varepsilon_F)$ is the density of states evaluated at the Fermi energy ε_F. (b) Thermal conductance G_T of the SM–EI junction vs. T. The curves correspond to $Z = 0, 1, 3, 5, 7$.

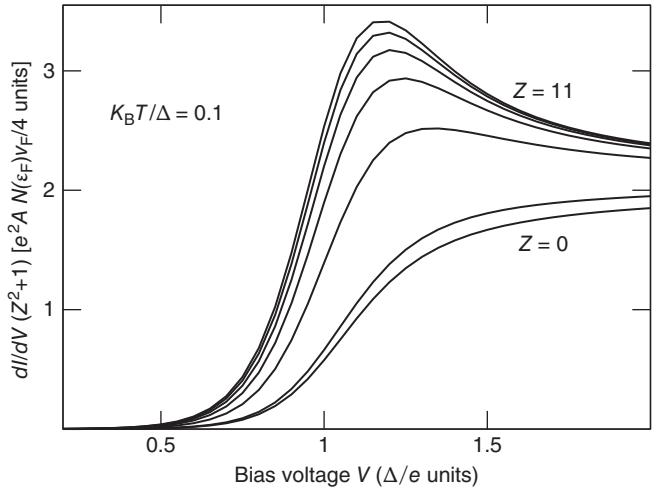

Fig. 19.7 Differential conductance $(dI/dV)/C_{\Delta=0}$ of the SM–EI junction vs bias voltage V, computed at $K_BT/\Delta = 0.1$. The curves correspond to different values of the dimensionless barrier opacity, $Z = 0, 1, 3, 5, 7, 9, 11$. For each value of Z, dI/dV is divided by the corresponding transmission coefficient when $\Delta = 0$, i.e., $C_{\Delta=0} = (Z^2 + 1)^{-1}$.

$$\dot{S} = G(\delta V)^2/T + \mathcal{A}G_T(\delta T)^2/T^2, \tag{19.45}$$

with δT and δV being respectively the temperature and voltage drops at the interface and $\mathcal{A}$ being the cross-sectional area. In the N–S junction the superfluid component does not carry any entropy. Therefore, the terms proportional to G and G_T only include the contribution of quasiparticles which, when they cross the N–S interface, experience the same electric and thermal resistance as electrons do across the SM–EI boundary.

To shed light on the dissipationless motion of electrons in the linear transport regime, we vary the opacity of the SM–EI junction. The coherence between the two sides of the interface is diminished as the dimensionless barrier strength Z increases from zero (clean junction) to finite values (tunneling regime). Figure 19.6 displays G and G_T for increasing values of Z. Since the transmission coefficient $C(\omega)$ decreases uniformly in the absence of any electron–hole pairing (cf. Table 19.2), $C_{\Delta=0} = (Z^2 + 1)^{-1}$, we rescale conductances dividing them by $C_{\Delta=0}$. Naively, we would expect that the insertion of an insulating layer would reduce the conductances. On the contrary, the effect is just the opposite: as Z increases, $G/C_{\Delta=0}$ and $G_T/C_{\Delta=0}$ *increase*, eventually reaching saturation in the tunneling regime. This shows that the exciton order induced in the SM side by EI makes the junction less conductive for charge and heat transport. The plot of the differential conductance $(dI/dV)/C_{\Delta=0}$ vs the bias voltage V at low T (Fig. 19.7) allows clear monitoring of the transition from the transparent to the opaque limit, where transport is recovered. The effect is maximum for $eV \approx \Delta$ and as $T \to 0$, when the differential conductance becomes proportional to $C(eV) + D(eV)$.

19.5.1 Charge versus exciton current

As anticipated at the end of Section 19.4.1, the transport features discussed above which distinguish the excitonic insulator from the normal insulating state may be explained by two alternate physical pictures. The conventional

view is that electrons below the energy gap cannot contribute to transport as they are backscattered by the gap barrier, Δ, formed by the proximity effect of the EI. The less conventional view is to make use of the analogy with the N–S junction. Instead of counting the electrons in the valence band as negatively charged carriers of the current, we may start with the state with the valence band filled to the top as carrying zero current even under an electrical or thermal current and regard each unoccupied state in the valence band as a positively charged carrier—a hole—moving in the direction opposite to the electron. Then the reflected electrons are replaced by incoming holes toward the barrier. Therefore, the incident conduction electron and the valence hole may be viewed as a correlated pair moving toward the interface [Fig. 19.4(a)]. The novelty is that a constant electron–hole current moves from the SM to the EI below the gap, where electric transport is blocked. As the electron–hole pair approaches the interface from the SM side, the *exciton* current is converted into the condensate *supercurrent*: the global effect is that in the steady state an exciton current exists flowing constantly and reversibly all the way from the SM to the EI without any form of dissipation.

The above scenario follows from the continuity equation for the electron–hole current. The probability density $\rho_{\text{e-h}}(\boldsymbol{r}, t)$ for finding either a conduction-band electron or a valence-band hole at a particular time and place is $\rho_{\text{e-h}}(\boldsymbol{r}, t) = |f|^2 + 1 - |g|^2$. Thus, the associated continuity equation is

$$\frac{\partial \rho_{\text{e-h}}}{\partial t} + \nabla \cdot \boldsymbol{J}_{\text{e-h}} = 0, \qquad \boldsymbol{J}_{\text{e-h}} = \boldsymbol{J}_{\text{pair}} + \boldsymbol{J}_{\text{cond}}. \tag{19.46}$$

One component of the electron–hole current,

$$\boldsymbol{J}_{\text{pair}} = \frac{1}{m} \text{Im}\left\{f^* \nabla f + g^* \nabla g\right\}, \tag{19.47}$$

is the density current of the electron–hole pair, similar to the standard particle carrier $\boldsymbol{J} = m^{-1}\text{Im}\{f^*\nabla f - g^*\nabla g\}$ with an important difference in sign. The other component,

$$\nabla \cdot \boldsymbol{J}_{\text{cond}} = -4\,\text{Im}\left\{f^* g\,\Delta\right\}, \tag{19.48}$$

depends explicitly on the built-in coherence of the electron–hole condensate Δ, and may be described as the exciton supercurrent of the EI state.

Let us go back to our picture of $\Delta(z)$ smoothly varying in space (Fig. 19.2), with the junction being divided into small neighborhoods at position $\boldsymbol{r}$ and each being a homogeneous system. If $\omega < |\Delta_0|$, each electron wave function, solution of Eq. (19.28), carries zero total electric current $e\boldsymbol{J}$, which is the sum of the equal and opposite incident and reflected fluxes, and finite and constant electron–hole current $\boldsymbol{J}_{\text{e-h}} = 2v_{\text{F}}\boldsymbol{n}$, with $\boldsymbol{n}$ a unit vector. When $z \to -\infty$, far from the interface on the SM side, the supercurrent contribution $\boldsymbol{J}_{\text{cond}}$ is zero. As z increases and $\Delta(z)$ gradually rises, both $\boldsymbol{J}$ and $\boldsymbol{J}_{\text{e-h}}$ conserve their constant value, independent of z, since quasiparticle states are stationary. However, their analysis in terms of incident and reflected quasiparticles is qualitatively different.

From the electron point of view, we see in Fig. 19.2(a) that the incoming conduction-band particle approaching the EI boundary sees its group velocity

progressively reduced (from time step 1 to time step 3), up to the classical turning point (time step 4) where it changes direction and branch of the spectrum: there is no net electric current.

From the exciton point of view, as the contribution to the electron–hole current $\boldsymbol{J}_{\text{pair}}$ vanishes approaching the boundary, since the group velocity goes to zero at the classical turning point where the wave function becomes evanescent, $\boldsymbol{J}_{\text{pair}}$ is converted into the supercurrent $\boldsymbol{J}_{\text{cond}}$. Excitons therefore can flow into the EI side without any resistance, and the sum $\boldsymbol{J}_{\text{e-h}}$ of the two contributions, $\boldsymbol{J}_{\text{pair}}$ and $\boldsymbol{J}_{\text{cond}}$, is constant through all the space [Fig. 19.4(a)].

As ω exceeds $|\Delta_0|$, $\boldsymbol{J}$ acquires a finite value and $\boldsymbol{J}_{\text{e-h}}$ monotonously decreases. However, close to the gap, electron transmission to the EI side is still inhibited [cf. Eq. (19.43)] by the pairing between electrons and holes of the condensate: an electron can stand alone and carry current only after its parent exciton has been "ionized" by injecting—say— a conduction-band electron or by filling a valence-band hole in the EI. The ionization costs an amount of energy of the order of the binding energy of the exciton, $|\Delta_0|$. Therefore, as long as $\omega \approx |\Delta_0|$, the competition between exciton and electron flow favors Andreev reflection, which is the source of both electric and thermal resistances.

In equilibrium, there is no net charge or heat flow, since quasi-particles with $\boldsymbol{v}$ and $-\boldsymbol{v}$ compensate each other. However, if a heat current flows, the net drift velocity of electrons and holes locally "drags" the exciton supercurrent, which otherwise would be pinned by various scattering sources [279].

19.5.2 A concrete example

As a concrete example of the aforementioned conversion of free-exciton current into condensate supercurrent, consider the quasiparticle steady state of Eq. (19.40). For $\omega < \Delta$, k^+ and k^- in the EI ($z > 0$) have small imaginary parts which lead to an exponential decay on a length scale λ, where

$$\lambda = \frac{v_{\text{F}}}{2\Delta}\left(1 - \frac{\omega^2}{\Delta^2}\right)^{-1/2}. \tag{19.49}$$

The quasiparticles penetrate a depth λ before the electron–hole current J_{pair} is converted to a supercurrent J_{cond} carried by the condensate; right at the gap edge the length diverges. For clarity, we define C and D here as the transmission probabilities at $z \gg \lambda$, while for $\omega > \Delta$ plane-wave currents are spatially uniform and we need not specify the position at which they are evaluated.

When the interface is transparent, $Z = 0$, the steady state (19.40) is specified by $b = d = 0$, $a = v_0/u_0$, and $c = 1/u_0$. Below the gap coherence factors u_0 and v_0 are complex and equal in modulus. For $\omega < \Delta$, $|a|^2 = 1$, which means the incident conduction-band electron is totally reflected into the SM valence band. Thus, the electron–hole current J_{pair} carried in the semimetal equals $2v_{\text{F}}$, but J_{pair} of the excitonic insulator is exponentially small for $z \gg 0$. Explicitly,

$$J_{\text{pair}} = \frac{|c|^2}{m}(|u_0|^2 + |v_0|^2)\,\text{Im}\left[(\text{e}^{\text{i}k^+z})^* \frac{\partial}{\partial z}(\text{e}^{\text{i}k^+z})\right].$$

Letting $k^+ \approx k_\mathrm{F} + \mathrm{i}/(2\lambda)$, we have

$$J_\mathrm{pair} = 2v_\mathrm{F}\mathrm{e}^{-z/\lambda}. \tag{19.50}$$

The "disappearing" electron–hole current reappears as exciton current carried by the condensate. Recalling the definition of J_cond,

$$\partial J_\mathrm{cond}/\partial z = -\,4\,\mathrm{Im}\{f^* g\,\Delta\},$$

by integration we obtain

$$J_\mathrm{cond} = -\,4\Delta\,|c|^2 \int_0^z \mathrm{d}\,z'\mathrm{e}^{-z'/\lambda}\,\mathrm{Im}\big[u_0^* v_0\big] = 2v_\mathrm{F}\left(1-\mathrm{e}^{-z/\lambda}\right). \tag{19.51}$$

This is the desired result, explicitly showing the supercurrent J_cond increasing to an asymptotic value as $z \to \infty$, at the same rate as the free electron–hole current J_pair dies away.

19.6 Josephson oscillations between exciton condensates in electrostatic traps

The Josephson effect is a macroscopic coherent phenomenon which has been observed in systems as diverse as superconductors [287], superfluid helium [288–290], and Bose–Einstein condensates of trapped ultra-cold atomic gases [291–294]. Since Josephson oscillations appear naturally when two spatially separated macroscopic wave functions are weakly coupled, they have been predicted for bosonic excitations in solids as well, like polaritons [295, 296] and excitons optically pumped in suitable semiconductor heterostructures [297]. However, unlike the polaritons, which have a photonic component allowing for easy detection, excitons stay dark unless they recombine radiatively. So far, it is unclear how the exciton Josephson effect could be observed. One proposal relied on the observation of quasiparticle excitations from the spectral properties of the emitted light [296]. A drawback of this idea is that spectral properties are not unambiguously linked to the condensed phase. In this section we propose the interference of emitted photons as a direct probe of the exciton Josephson effect.

Condensed excitons are predicted to act as coherent light sources [127–129] (see discussion below). If Josephson oscillations occur between two exciton traps, in principle they can be probed by measuring the interference of the beams separately emitted from the traps. However, in the time interval before recombination and contrary to the polariton case, there are too few photons emitted for an adequate signal to noise ratio, so one has to average the signal over many replicas of the same experiment [40]. Here we show that such ensemble averaging blurs the signature of the Josephson effect except in the relevant case of exciton "plasma" oscillations [16]. For the latter the dipole energy difference between the traps modulates the visibility α of interference fringes, providing a means for detection.

The subsections below are organized as follows: we first introduce the double quantum well system illustrating a feasible scheme to manipulate

electrically the exciton phase (Section 19.6.1); we then set the theoretical framework (Section 19.6.2), and we eventually propose a correlated photon counting experiment (Section 19.6.3).

19.6.1 Electrical control of the exciton phase

Consider a double quantum well where electrons and holes are separately confined in the two layers. In experiments aiming at Bose–Einstein condensation of excitons, electron–hole pairs are optically generated at energies higher than the band gap, left to thermalize, form excitons, and, at sufficiently low temperature and high density, condense before radiative decay [26, 40]. Let z be the growth axis of the two wells separated by distance d. The electrons in the conduction band and holes in the valence band move in the planes $z = d$, 0, respectively (Fig. 19.8). In the experiments [24, 25], an electric field F_z is applied along z to suppress inter-layer tunneling, thereby quenching the exciton recombination.

Fabrications [83, 84, 96] of electrostatic traps with suitably located electrodes to provide lateral confinement for the excitons have been implemented. The double quantum well is sandwiched between two spacer layers, providing insulation from planar electrodes lithographed on both sides of the coupled structure. Each electrode controls a tunable gate voltage, $V_g(x, y, z)$, which localizes in a region of the xy plane the field component along z, $F_z(x, y, z) = -\partial V_g(x, y, z)/\partial z$, while F_x and F_y are small and can be neglected as well as the dependence of F_z on z. The vertical field $F_z(x, y)$ makes the electrostatic potential energy of the exciton dipole depend on the lateral position, $U_X(x, y) = -edF_z(x, y)$ ($e < 0$) [cf. Fig. 19.8(b)]. In this way, potential traps for excitons are designed with great flexibility, with *in situ* control of the height, width, and shape of the potential barriers [83, 88].

First, we focus on the quasi-equilibrium situation before radiative recombination, where excitons condense in two coupled electrostatic traps, both within the condensate coherence length. Figure 19.8(b) depicts the exciton potential profile $U_X(x, y = 0)$ along the x axis, with a link between two identical traps. The potential barrier allows tunneling between the condensates in the two traps, whose macroscopic wave functions are $\Xi_1(x, y, t)$ and $\Xi_2(x, y, t)$, respectively. The optical coherence in a single trap is of the form

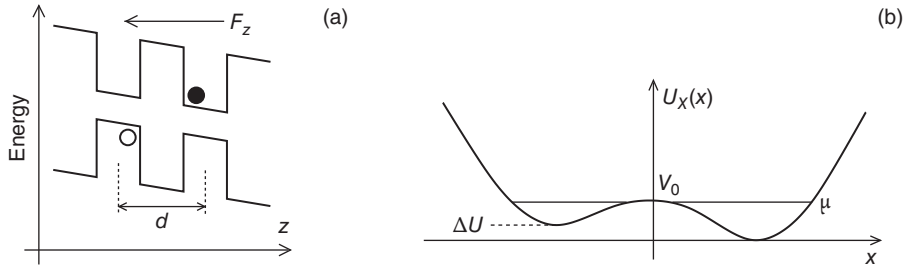

Fig. 19.8 (a) Double quantum well energy profile along the growth direction z. Electrons and hole move freely in the xy planes at $z = d$ and $z = 0$, respectively. F_z is the component of the electric field parallel to the exciton electric dipole. (b) Effective exciton potential profile vs. x for the double-trap setup.

$$\Xi(x,y,t) = \left\langle \Psi_a^\dagger(x,y,0,t)\Psi_b(x,y,d,t)\right\rangle, \tag{19.52}$$

where $\langle \ldots \rangle$ denotes quantum and thermal average in the grand canonical formalism. In Eq. (19.52) $\Psi_a^\dagger(x,y,0,t)$ and $\Psi_b(x,y,d,t)$ are respectively the hole and electron destruction operators, with the vacuum being the semiconductor ground state with no excitons. With respect to definition (19.13), here by putting $(x,y) = (x',y')$ we ignore the internal structure of the exciton relative-motion wave function. The reason is that we focus on the ideal BEC limit of dilute weakly interacting excitons, $n\,a_{\rm B}^2 \ll 1$, with $a_{\rm B}$ being the two-dimensional effective Bohr radius and n the exciton density. Therefore, $\Xi(x,y,t)$ is the macroscopic wave function for the center-of-mass motion of excitons, which may be written in the form

$$\Xi(x,y,t) = \sqrt{n_s}\, e^{\mathrm{i}\varphi}, \tag{19.53}$$

with n_s being the density of the exciton condensate and φ the phase. We recall that only the relative phase between the two condensates has measurable effects [298, 299].

For a gauge transformation of the gate potential $V_g \to V_g - c^{-1}\partial\chi(t)/\partial t$, which leaves the field F_z unaltered, the field operators Ψ gain a phase,

$$\begin{aligned}\Psi_a &\to \Psi_a \exp\left[\frac{\mathrm{i}e}{\hbar c}\,\chi(x,y,0,t)\right],\\ \Psi_b &\to \Psi_b \exp\left[\frac{\mathrm{i}e}{\hbar c}\,\chi(x,y,d,t)\right].\end{aligned} \tag{19.54}$$

Throughout this section we indicate explicitly the reduced Planck's constant $\hbar$. The macroscopic wave function, by Eq. (19.52), also gains a phase,

$$\varphi \to \varphi + \frac{e}{\hbar c}\left[\chi(z=d,t) - \chi(z=0,t)\right]. \tag{19.55}$$

Hence, the frequency of time oscillation of the condensate is given by the electrostatic energy of the exciton dipole in the external field [219], $U = -edF_z$:

$$\varphi = \varphi^{(0)} + \frac{1}{\hbar} edF_z t, \tag{19.56}$$

with $\varphi^{(0)}$ being the time-independent zero-field value. In the absence of the bilayer separation of the electrons and the holes, their gauge phases gained in the electric field would cancel each other resulting in no time dependence driven by U. Equation (19.56) shows that the experimentally controllable dipole energy difference between the two traps depicted in Fig. 19.8(b), $\Delta U = -ed(F_{z1} - F_{z2})$, drives the relative phase between the two condensates, thereby creating Josephson oscillations as a means for measuring the Josephson tunnel between the traps.

19.6.2 Exciton Josephson oscillations

We next introduce the usual two-mode description of inter-trap dynamics based on the Gross–Pitaevskii (GP) equation [16, 295–297, 300–302]. Exciton–exciton correlation [303] beyond the GP mean field may be neglected due to

the repulsive character of the dipolar interaction between excitons in coupled quantum wells. The condensate total wave function solution is

$$\Xi(x, y, t) = \Xi_1(x, y, N_1)\, e^{i\varphi_1} + \Xi_2(x, y, N_2)\, e^{i\varphi_2}, \tag{19.57}$$

where both the trap population $N_i(t)$ and the condensate phase $\varphi_i(t)$ possess the entire time dependence for the ith trap ($i = 1, 2$), and $\Xi_i(x, y, N_i)$ is a real quantity, with

$$\int dx \int dy\ \Xi_i^2(x, y, N_i) = N_i(t). \tag{19.58}$$

The dynamics of the GP macroscopic wave function $\Xi(x, y, t)$ depends entirely on the temporal evolution of two variables, the population imbalance $k(t) = (N_1 - N_2)/2$ and the relative phase $\phi(t) = \varphi_1 - \varphi_2$ of the two condensates. Here we consider a time interval much shorter than the exciton lifetime (10—100 ns) and ignore the spin structure. Therefore, the total population is approximately constant, $N_1(t) + N_2(t) = N$.

The equations of motion for the canonically conjugated variables $\hbar k$ and ϕ are derived from the effective hamiltonian

$$H_J = E_c \frac{k^2}{2} + \Delta U k - \frac{\delta_J}{2}\sqrt{N^2 - 4k^2}\cos\phi, \tag{19.59}$$

under the condition $k \ll N$ ([16]). $E_c = 2d\mu_1/dN_1$ is the exciton "charging" energy of one trap, where μ_1 is the chemical potential of trap 1, whereas δ_J is the Bardeen single-particle tunneling energy,

$$\delta_J = \frac{\hbar^2}{m}\int dy \left[\xi_1\left(\frac{\partial \xi_2}{\partial x}\right) - \xi_2\left(\frac{\partial \xi_1}{\partial x}\right)\right]_{x=0}, \tag{19.60}$$

where m is the exciton mass. The single-particle orbital $\xi_i(x, y)$ is defined through $\Xi_i(x, y) = \sqrt{N_i}\,\xi_i(x, y)$.

The various dynamical regimes associated to certain initial conditions $(k(0), \phi(0))$, including π oscillations and macroscopic quantum self-trapping, are exhaustively discussed in [300, 301]. Two cases are specially relevant:

19.6.2.1 *AC Josephson effect*

Under the conditions $\Delta U \gg NE_c/2$, $\Delta U \gg \delta_J$, one easily obtains

$$\phi(t) = -\frac{\Delta U}{\hbar}t + \phi(0), \qquad \dot{k} = \frac{\delta_J N}{2\hbar}\sin\phi. \tag{19.61}$$

Equation (19.61) shows that, analogous to the case of two superconductors separated by a thin barrier, if the phase difference ϕ between the condensates is not a multiple of π, an exciton supercurrent $2\dot{k}$ flows across the barrier. Remarkably, in the presence of an electric field gradient along z, an exciton flux oscillates back and forth between the two traps, with frequency $\Delta U/\hbar$. As an exciton goes through the barrier, it exchanges with the field the dipole energy acquired or lost in the tunneling process. The analogy with the AC Josephson effect for superconductors is clear: in that case a bias voltage V is applied across the junction, and the energy $2eV$ is exchanged between field and Cooper pairs, as the latter experience a potential difference of V when penetrating the potential barrier.

19.6.2.2 *Plasma oscillations*

This case concerns small oscillations around the equilibrium position $(k, \phi)_{\rm eq} = (0, 0)$. The hamiltonian (19.59) may then be linearized into the form

$$H_J = \frac{k^2}{2}\left(2\frac{\delta_J}{N} + E_c\right) + \frac{1}{4}\delta_J N\phi^2 + \Delta U k - \frac{\delta_J N}{2}. \tag{19.62}$$

It follows that both k and ϕ oscillate in time with plasma frequency

$$\omega_J = \frac{1}{\hbar}\sqrt{\delta_J(NE_c/2 + \delta_J)}. \tag{19.63}$$

Note that ΔU displaces the equilibrium position from $(k, \phi)_{\rm eq} = (0, 0)$ to

$$(k, \phi)_{\rm eq} = (-\Delta U N\delta_J/2(\hbar\omega_J)^2, 0). \tag{19.64}$$

19.6.3 Correlated photon counting experiment

Figure 19.9 illustrates the correlated photon counting setup which we propose to probe Josephson oscillations. The detector measures the intensity $I(\tau)$ of the sum of the two beams separately emitted from the traps. A delay time τ is induced in one of the two beams, as in [123]. The fields are simply proportional to the order parameters Ξ_i of the traps. In fact, $\Xi(x, y, t)$ is associated with a macroscopic electric dipole moment,

$$\boldsymbol{P}(t) = \hat{\boldsymbol{x}}P_x(t) \pm i\hat{\boldsymbol{y}}P_y(t), \tag{19.65}$$

which couples to photons:

$$P_x(t) = \int dx\, dy\, x\, \Xi(x, y, t), \tag{19.66}$$

and similarly for P_y. The built-in dipole $\langle \boldsymbol{P}(t)\rangle \neq 0$ oscillates with frequency $(\mu + E_X)/\hbar$, where E_X is the optical gap minus the exciton binding energy, and μ accounts for exciton–exciton interaction [127–129]. This macroscopic oscillating dipole is equivalent to a noiseless current, which radiates a coherent field [304].

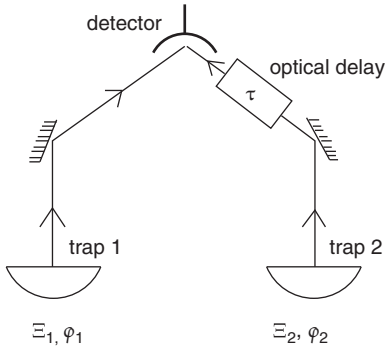

Fig. 19.9 Proposed experimental setup to measure the time correlation of the photons emitted from the two traps. The delay time τ of one optical path is externally controlled.

Therefore, the measured intensity $I(\tau)$ is

$$I(\tau) = 2I_0\left[1 + \langle\cos\phi(\tau)\rangle\right], \tag{19.67}$$

assuming that the fields emitted from the two traps have the same magnitude (and intensity I_0) but different relative phase ϕ, which is evaluated at the delayed time τ. $I(\tau)$ may be written as

$$I(\tau) = 2I_0\left[1 + \alpha\cos\phi_0(\tau)\right], \tag{19.68}$$

where $\phi_0(\tau)$ is the phase averaged over many measurements, defined by the condition

$$\langle\sin\left[\phi(\tau) - \phi_0(\tau)\right]\rangle = 0, \tag{19.69}$$

and

$$\alpha = \langle\cos\left[\phi(\tau) - \phi_0(\tau)\right]\rangle \tag{19.70}$$

is the fringe visibility, i.e., the normalized peak-to-valley ratio of fringes,

$$\alpha = \frac{I_{\max} - I_{\min}}{I_{\max} + I_{\min}}, \tag{19.71}$$

with $I_{\max}$ ($I_{\min}$) being the maximum (minimum) value of $I(\tau)$, and $0 \leq \alpha \leq 1$.

Equation (19.68) has a few important caveats. Since $I(\tau)$ is an average, the temporal inhomogeneous effect will blur the interference fringes, i.e., $\alpha < 1$. Other dephasing mechanisms include exciton recombination and inelastic exciton–phonon scattering [123], as well as inelastic [123] and elastic exciton–exciton scattering, which in first instance may all be neglected for short τ, low T, and $n a_B^2 \ll 1$, respectively.

The most immediate caveat is that the exciton condensates in decoupled traps must acquire a relative phase if initially they condense separately without a definite phase relation. This scenario is analogous to the case of interference between independent laser sources first discussed by Glauber [304] and later studied experimentally for matter waves [305]. Even though a one-shot measurement with sufficient resolution would display fringes, the relative phase $\phi_0(\tau)$ is also subject to intrinsic dephasing effects by quantum fluctuations [304]. The latter are significant noise sources which affect α, when ϕ and k are quantized into canonically conjugated quantum variables whereas in the GP theory used so far they were classical variables whose fluctuations where neglected.

In the following, we quantize hamiltonian (19.59) in order to properly evaluate $\alpha = \langle \cos[\phi(\tau) - \phi_0(\tau)] \rangle$ as a quantum statistical average in finite traps. Therefore, we follow [306] and introduce the commutator

$$\left[\hat{\phi}, \hat{k}\right] = i. \tag{19.72}$$

The operator $\hat{k}$ now appearing in the quantized version of hamiltonian (19.59) takes the form $-i\partial/\partial\phi$, whereas the ground-state wave function is defined in the space of periodical functions of ϕ with period 2π. If condensate oscillations are mainly coherent, the variance of ϕ is small and the visibility is approximated by $\alpha = 1 - \frac{1}{2}\left\langle (\Delta\phi)^2 \right\rangle$.

The most interesting case concerns plasma oscillations. For $\Delta U = 0$, the ground state of the quantized version of the harmonic oscillator hamiltonian (19.62) is a Gaussian, with $\phi_0 = 0$, independent from τ, and minimal spreading $\left\langle \Delta\phi^2 \right\rangle \approx (E_c/2\delta_J N)^{1/2}$. Therefore, the interferometer output is time-independent, $I = 2I_0(1 + \alpha)$, showing constructive interference, $I > 2I_0$, with

$$\alpha = 1 - \sqrt{\frac{E_c}{8\delta_J N}}. \tag{19.73}$$

Not surprisingly, the visibility is controlled by the ratio $E_c/\delta_J N$, reaching the maximum $\alpha = 1$ as $E_c/\delta_J N \to 0$. In fact, α is given by the balance between the competing effects of tunneling ($\propto \delta_J N$), which enforces a well-defined inter-trap phase, and inverse compressibility ($\propto E_c$), which favors the formation of separate number states in the two traps, thus separating the two macroscopic wave functions.

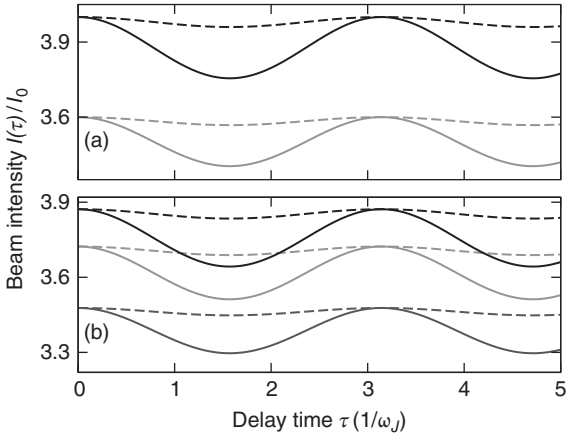

Fig. 19.10 Beam intensity $I(\tau)/I_0$ vs. delay time τ, for $\Delta U/\hbar\omega_J = 0.2, 0.5$ (dashed and solid lines, respectively). (a) $T = 0$ and $\alpha = 1$, 0.8 (black and light gray lines, respectively). (b) $\alpha(T = 0) = 0.94$ and $k_BT/\hbar\omega_J = 0$, 1, 2 (black, light gray, and dark gray lines, respectively).

A small finite value of ΔU in Eq. (19.62) displaces the equilibrium position of the harmonic oscillator. Noticeably, the ground state is a *coherent* state with harmonic evolution of the average phase in time,

$$\phi_0(\tau) = -\frac{\Delta U}{\hbar\omega_J}\sin(\omega_J\,\tau), \tag{19.74}$$

whereas α is unchanged. The Gaussian probability density characteristic of the ground state for $\Delta U = 0$ now is simply carried back and forth in ϕ space in the same motion as the expectation value $\phi_0(\tau)$.

This key feature allows for directly monitoring τ-dependent plasma oscillations of frequency ω_J through the photon correlation measurement (cf. Fig. 19.10). We evaluate the effect of thermal fluctuations on α via the formula

$$\alpha(T) = \frac{\sum_n \alpha_n \exp[-\beta E_n]}{\sum_n \exp[-\beta E_n]}, \tag{19.75}$$

where $\beta = 1/k_BT$ and $2(\alpha_n - 1) = \langle(\Delta\phi)^2\rangle_n$ is the variance of ϕ in the nth excited state whose energy is E_n. At low T, the excited states may be approximated as those of the harmonic oscillator, giving

$$\alpha(T) = 1 - \sqrt{\frac{E_c}{2\delta_J N}}\left(\frac{1}{2} + \frac{1}{e^{\beta\hbar\omega_J} - 1}\right). \tag{19.76}$$

The above results are summarized by the formula

$$I(\tau) = 2I_0\left[1 + \alpha(T)\cos\left(\frac{\Delta U}{\hbar\omega_J}\sin\omega_J\,\tau\right)\right], \tag{19.77}$$

which is valid for $E_c/\delta_J N \ll 1$.

For small dipole energy variations, $\Delta U/\hbar\omega_J \ll 1$, the oscillating part within the square brackets of Eq. (19.77) may be written as $-\alpha(T)/2(\Delta U/\hbar\omega_J)^2\sin^2\omega_J\,\tau$. This shows that the visibility $\alpha(T)$ of fringes, which oscillate like $\sin^2\omega_J\,\tau$, is modulated by the experimentally tunable factor $(\Delta U/\hbar\omega_J)^2/2$. The dependence of $I(\tau)$ on ΔU is illustrated in Fig. 19.10

for two values of $\Delta U/\hbar\omega_J$. As $\Delta U/\hbar\omega_J$ is increased [from 0.2 (dashed lines) to 0.5 (solid lines)], the amplitude of oscillations of $I(\tau)$ shows a strong nonlinear enhancement, providing a clear signature of Josephson oscillations. The oscillation amplitudes are larger for higher values of α [cf. Fig. 19.10(a)], and fairly robust against thermal smearing [cf. Fig. 19.10(b)]. In fact, Fig. 19.10(b) shows that the oscillation of $I(\tau)$ is still clearly resolved for temperatures as high as $T \approx \hbar\omega_J/k_B$. At even higher temperatures $\alpha(T)$ displays anharmonic effects [306], with $\alpha(T) \to 0$ as $T \to \infty$.

The a.c. Josephson effect cannot be observed within our scheme. In fact, for large values of ΔU, the term proportional to $\cos\phi$ appearing in the hamiltonian (19.59) may be neglected in first approximation, and the ground-state wave function is a plane wave, $(2\pi)^{-1/2}\exp[i\bar{n}\phi]$, where $\bar{n}$ is the integer closest to $-\Delta U/E_c$. Since the probability density, $(2\pi)^{-1}$, is constant, the phase is distributed randomly and the visibility is zero. Therefore, the correction to α coming from the inclusion in the calculation of the term neglected in Eq. (19.59) will be small and fragile against fluctuations.

19.7 Conclusions

The venerated topic of exciton Bose–Einstein condensation is facing a rebirth as its investigation is fueled by advances in novel materials and technologies, as for double-layer semiconductors and graphene. Indeed, growing evidence shows that the concept of exciton condensation is a paradigm of many-body behavior. The observation of the coherence properties of the condensate, including superfluidity, is an important long-term goal of this field. In this chapter we have explained how the exciton analogs of Andreev reflection and Josephson oscillations may be linked to measurable quantities. We hope that these ideas may stimulate further experiments along this path.

Acknowledgments

We thank Leonid Butov for critically reading the manuscript. This work is supported by EU-FP7 Marie Curie Initial Training Network "Indirect Excitons: Fundamental Physics and Applications (INDEX)".

References

[1] Knox R. S. *Theory of Excitons*, Volume Supplement 5, Solid State Physics Academic Press, New York (1963).

[2] Rashba E. I. and Sturge M. D. *Excitons*, North-Holland, Amsterdam (1982).

[3] Schäfer W. and Wegener M. *Semiconductor Optics and Transport Phenomena*, Springer, Berlin (2002).

[4] Shah J. *Ultrafast Spectroscopy of Semiconductors and Semiconductor Nanostructures* (Second edn). Springer, Berlin (1999).

[5] Yu P. Y. and Cardona M. *Fundamentals of Semiconductors* (Third edn), Springer, Berlin (2004).

[6] Sham L. J. and Rice T. M. Many-particle derivation of the effective-mass equation for the Wannier exciton, *Phys. Rev.* **144**, 708 (1966).

[7] Blatt J. M., Böer K. W., and Brandt W. Bose-Einstein condensation of excitons, *Phys. Rev.* **126**, 1691 (1962).

[8] Moskalenko S. A. Reversible optico-hydrodynamic phenomena in a nonideal exciton gas, *Fiz. Tverd. Tela.* **4**, 276 (1962). [Sov. Phys. Solid State **4**, 199 (1962)].

[9] Casella R. C. On the possibility of observing a Bose-Einstein condensation of excitons in CdS and CdSe, *J. Phys. Chem. Solids* **24**, 19 (1963).

[10] Keldysh L. V. and Kozlov Z. N. Collective properties of large-radius excitons, *Zh. Eksp. i Teor. Fiz. Pisma* **5**, 238 (1967). [Sov. Phys.–JETP Lett. **5**, 190 (1968)].

[11] Agranovich V. M. and Toshich B. S. Collective properties of Frenkel excitons, *Zh. Eksp. i Teor. Fiz.* **53**, 149 (1967). [Sov. Phys.–JETP **26**, 104 (1968)].

[12] Keldysh L. V. and Kozlov A. N. Collective properties of excitons in semiconductors, *Zh. Eksp. i Teor. Fiz.* **54**, 978 (1968). [Sov. Phys.–JETP **27**, 521 (1968)].

[13] Gergel', V. A., Kazarinov R. F., and Suris R. A. Superfluidity of excitons in semiconductors, *Zh. Eksp. i Teor. Fiz.* **54**, 298 (1968). [Sov. Phys.–JETP **27**, 159 (1968)].

[14] Comte C. and Nozières P. Exciton Bose condensation: the ground state of an electron-hole gas – I. Mean field description of a simplified model, *J. Phys.* **43**, 1069 (1982).

[15] Griffin A., Snoke D. W., and Stringari S. (ed.) *Bose-Einstein Condensation*. Cambridge University Press, Cambridge (UK) (1995).

[16] Pitaevskii L. and Stringari S. *Bose-Einstein Condensation*, Oxford University Press, Oxford (2003).

[17] Hanamura E. and Haug H. Condensation effects of excitons, *Phys. Rep.* **33**, 209 (1977).

[18] Mysyrowicz A. Excitons as a new quantum system, *J. Phys. Colloques*, **41**(C7), 281 (1980).

[19] Littlewood P. B. and Zhu X. Possibilities for exciton condensation in semiconductor quantum-well structures, *Phys. Scripta* **T68**, 56 (1996).

[20] Moskalenko S. A. and Snoke D. W. *Bose-Einstein Condensation of Excitons and Biexcitons*. Cambridge University Press, Cambridge (2000).

[21] Larionov A. V. and Timofeev V. B. Condensation of interwell excitons in GaAs/AlGaAs double quantum wells, *JETP Lett.* **73**, 301 (2001).

[22] Snoke D. Spontaneous Bose coherence of excitons and polaritons, *Science* **298**, 1368 (2002)

[23] Butov L. V. Exciton condensation in coupled quantum wells, *Solid State Commun.* **127**, 89 (2003).

[24] Butov L. V. Condensation and pattern formation in cold exciton gases in coupled quantum wells, *J. Phys.: Condens. Matter* **16**, R1577 (2004).

[25] Butov L. V. Cold exciton gases in coupled quantum well structures, *J. Phys.: Condens. Matter* **19**, 295202 (2007).

[26] Ivanov A. L. and Tikhodeev S. G. (ed.) *Problems of Condensed Matter Physics: Quantum Coherence Phenomena in Electron-Hole and Coupled Matter-Light Systems*. Oxford University Press, Oxford (2008).

[27] Snoke D. W. Coherence and optical emission from bilayer exciton condensates, *Adv. in Condens. Matter Phys.* **2011**, 938609 (2011).

[28] Rice T. M. The electron-hole liquid in semiconductors: Theoretical aspects, *Solid State Phys.* **32**, 1 (1977).

[29] Keldysh L. V. The electron-hole liquid in semiconductors, *Contemp. Phys.* **27**, 395 (1986).

[30] Hulin D., Mysyrowicz A., and Benoît à la Guillame C. Evidence for Bose-Einstein statistics in an exciton gas, *Phys. Rev. Lett.* **45**, 1970 (1980).

[31] Shevchenko S. I. Theory of superconductivity of systems with pairing of spatially separated electrons and holes, *Fiz. Nizk. Temp.* **2**, 505 (1976). [Sov. J. Low Temp. Phys. **2**, 251 (1976)].

[32] Lozovik Yu. E. and Yudson V. I. A new mechanism for superconductivity: pairing between spatially separated electrons and holes, *Zh. Eksp. i Teor. Fiz.* **71**, 738 (1976). [Sov. Phys.–JETP **44**, 389 (1976)].

[33] Fukuzawa T. and Kano S. S. Possibility of coherent light emission from Bose condensed states of SEHPs, *Surf. Sci.* **228**, 482 (1990).

[34] Alexandrou A., Kash J. A., Mendez E. E., Zachau M., Hong J. M., Fukuzawa T., and Hase Y. Electric-field effects on exciton lifetimes in symmetric coupled GaAs/$Al_{0.3}Ga_{0.7}$As double quantum wells, *Phys. Rev. B* **42**, 9225(R) (1990).

[35] Zrenner A., Leeb P., Schäfler J., Böhm G., Weimann G., Worlock J. M., Florez L. T., and Harbison J. P. Indirect excitons in coupled quantum well structures, *Surf. Sci.* **263**, 496 (1992).

[36] Butov L. V., Gossard A. C., and Chemla D. S. Macroscopically ordered state in an exciton system, *Nature* **418**, 751 (2002).

[37] Snoke D., Denev S., Liu Y., Pfeiffer L., and West K. Long-range transport in excitonic dark states in coupled quantum wells, *Nature* **418**, 754 (2002).

[38] Butov L. V., Levitov L. S., Mintsev A. V., Simons B. D., Gossard A. C., and Chemla D. S. Formation mechanism and low-temperature instability of exciton rings, *Phys. Rev. Lett.* **92**, 117404 (2004)

[39] Rapaport R., Chen G., Snoke D., Simon S. H., Pfeiffer L., West K., Liu Y., and Denev S. Charge separation of dense two-dimensional electron-hole gases: Mechanism for exciton ring pattern formation, *Phys. Rev. Lett.* **92**, 117405 (2004).

[40] High A. A., Leonard J. R., Hammack A. T., Fogler M. M., Butov L. V., Kavokin A. V., Campman K. L., and Gossard A. C. Spontaneous coherence in a cold exciton gas, *Nature* **483**, 584 (2012).

[41] Timofeev V. B. and Gorbunov A. V. Collective state of the Bose gas of interacting dipolar excitons, *J. Appl. Phys.* **101**, 081708 (2007).

[42] Mott N. F. The transition to the metallic state, *Phil. Mag.* **6**(8), 287 (1961).

[43] Keldysh L. V. and Kopaev Yu V. Possible instability of the semimetallic state against Coulomb interaction, *Fiz. Tverd. Tela.* **6**, 2791 (1964). [Sov. Phys. Solid State **6**, 2219 (1965)].

[44] des Cloizeaux J. Exciton instability and crystallographic anomalies in semiconductors, *J. Phys. Chem. Solids* **26**, 259 (1965).

[45] Jèrome D., Rice T. M., and Kohn W. Excitonic insulator, *Phys. Rev.* **158**, 462 (1967).

[46] Bardeen J., Cooper L. N., and Schrieffer J. R. Theory of superconductivity, *Phys. Rev.* **108**, 1175 (1957).

[47] Halperin B. I. and Rice T. M. The excitonic state at the semiconductor-semimetal transition, *Solid State Phys.* **21**, 115 (1968).

[48] Kohn W. *Many-Body Physics*, p. 351, Gordon and Breach, New York (1968).

[49] Nozières P. and Comte C. Exciton Bose condensation: The ground state of an electron-hole gas – II. Spin states, screening and band structure effects, *J. Phys*. **43**, 1083 (1982).

[50] Littlewood P. B., Eastham P. R., Keeling J. M. J., Marchetti F. M., Simons B. D., and Szymanksa M. H. Models of coherent exciton condensation, *J. Phys.: Condens. Matter* **16**, S3597 (2004).

[51] Leggett A. J, *Quantum Liquids* (1st edn). Oxford University Press, Oxford (2006).

[52] Bloch I., Dalibard J., and Zwerger W. Many-body physics with ultracold gases, *Rev. Mod. Phys.* **80**, 885 (2008).

[53] Giorgini S., Pitaevskii L. P., and Stringari S. Theory of ultracold atomic Fermi gases, *Rev. Mod. Phys.* **80**, 1215 (2008).

[54] Ginzburg V. L. and Kirzhnits D. A. On the superfluidity of neutron stars, *Zh. Eksp. i Teor. Fiz. Pisma* **47**, 2006 (1964). [Sov. Phys.–JETP **20**, 1346 (1965)].

[55] Pines D., Baym G., and Pethick C. Superfluidity in neutron stars, *Nature*, **224**, 673 (1969).

[56] de Gennes P. G, *Superconductivity of Metals and Alloys*. Westview Press, Boulder (Colorado) (1999).

[57] Migdal A. B. Superfluidity and the moments of inertia of nuclei, *Zh. Eksp. i Teor. Fiz. Pisma* **37**, 249 (1959). [Sov. Phys.–JETP **10**, **176**, (1960)].

[58] Bohr A. and Mottelson B. R, *Nuclear Structure — Vol. I and II*, World Scientific, Singapore (1998).

[59] Rontani M. and Sham L. J. Coherent transport in a homojunction between an excitonic insulator and semimetal, *Phys. Rev. Lett.* **94**, 186404 (2005).

[60] Rontani M. and Sham L. J. Variable resistance at the boundary between semimetal and excitonic insulator, *Solid State Commun.* **134**, 89 (2005).

[61] Rontani M. and Sham L. J. Josephson oscillations between exciton condensates in electrostatic traps, *Phys. Rev. B* **80**, 075309 (2009).

[62] Kohn W. and Sherrington D. Two kinds of bosons and Bose condensates, *Rev. Mod. Phys.* **42**, 1 (1970).

[63] Zittartz J. Transport properties of the "excitonic insulator": Electrical conductivity, *Phys. Rev.* **165**, 605 (1968).

[64] Zittartz J. Transport properties of the "excitonic insulator": Thermal conductivity, *Phys. Rev.* **165**, 612 (1968).

[65] Kavoulakis G. M. BoseEinstein condensation of indirect excitons in coupled quantum wells, *J. Low Temp. Phys.* **132**, 297 (2003).

[66] Kuwata-Gonokami M. *Comprehensive Semiconductor Science and Technology*, Volume 2, p. 213. Elsevier, Amsterdam, The Netherlands (2011).

[67] Schwartz R., Naka N., Kieseling F., and Stolz H. Dynamics of excitons in a potential trap at ultra-low temperatures: Paraexcitons in Cu_2O, *New J. Phys.* **14**, 023054 (2012).

[68] Zhao W., Stenius P., and İmamoğlu A. Kinetics of condensation in trapped exciton gases, *Phys. Rev. B* **56**, 5306 (1997).

[69] Butov L. V., Zrenner A., Abstreiter G., Böhm G., and Weimann G. Condensation of indirect excitons in coupled AlAs/GaAs quantum wells, *Phys. Rev. Lett.* **73**, 304 (1994).

[70] Stern M., Gardimer V., Umansky V., and Bar-Joseph I. Mott transition of excitons in coupled quantum wells, *Phys. Rev. Lett.* **100**, 256402 (2008).

[71] Schindler C. and Zimmermann R. Analysis of the exciton-exciton interaction in semiconductor quantum wells, *Phys. Rev. B* **78**, 045313 (2008).

[72] Vögele X. P., Schuh D., Wegscheider W., Kotthaus J. P., and Holleitner A. W. Density enhanced diffusion of dipolar excitons within a one-dimensional channel, *Phys. Rev. Lett.* **103**, 126402 (2009).

[73] Lee R. M., Drummond N. D., and Needs R. J. Exciton-exciton interaction and biexciton formation in bilayer systems, *Phys. Rev. B* **79**, 125308 (2009).

[74] Vörös Z., Snoke D. W., Pfeiffer L. N., and West K. Direct measurement of exciton-exciton interaction energy, *Phys. Rev. Lett.*, **103**, 016403 (2009).

[75] Cohen K., Rapaport R., and Santos P. V. Remote dipolar interactions for objective density calibration and flow control of excitonic fluids, *Phys. Rev. Lett.* **106**, 126402 (2011).

[76] Ivanov A. L. Quantum diffusion of dipole-oriented indirect excitons in coupled quantum wells, *Europhys. Lett.* **59**, 586 (2002).

[77] Savona V. Effect of interface disorder on quantum well excitons and microcavity polaritons, *J. Phys.: Condens. Matter* **19**, 295208 (2007).

[78] High A. A., Hammack A. T., Butov L. V., Mouchliadis L., Ivanov A. L., Hanson M., and Gossard A. C. Indirect excitons in elevated traps, *Nano Lett.* **9**, 2094 (2009).

[79] High A. A., Thomas A. K., Grosso G., Remeika M., Hammack A. T., Meyertholen A. D., Fogler M. M., Butov L. V., Hanson M., and Gossard A. C. Trapping indirect excitons in a GaAs quantum-well structure with a diamond-shaped electrostatic trap, *Phys. Rev. Lett.* **103**, 087403 (2009).

[80] Remeika M., Graves J. C., Hammack A. T., Meyertholen A. D., Fogler M. M., Butov L. V., Hanson M., and Gossard A. C. Localization-delocalization transition of indirect excitons in lateral electrostatic lattices, *Phys. Rev. Lett.* **102**, 186803 (2009).

[81] Alloing M., Lemaître A., and Dubin F. Quantum signature blurred by disorder in indirect exciton gases, *Europhys. Lett.* **93**, 17007 (2011).

[82] Huber T., Zrenner A., Wegscheider W., and Bichler M. Electrostatic exciton traps, *Phys. Status Solidi A* **166**, R5 (1998).

[83] Hammack A. T., Gippius N. A., Yang S., Andreev G. O., Butov L. V., Hanson M., and Gossard A. C. Excitons in electrostatic traps, *J. Appl. Phys.* **99**, 066104 (2006).

[84] Chen G., Rapaport R., Pfeiffer L. N., West K., Platzman P. M., Simon S., Vörös Z., and Snoke D. Artificial trapping of a stable high-density dipolar exciton fluid, *Phys. Rev. B* **74**, 045309 (2006).

[85] Gorbunov A. V. and Timofeev V. B. Large-scale coherence of the Bose condensate of spatially indirect excitons, *JETP Lett.* **84**, 329 (2006).

[86] Gärtner A., Prechtel L., Schuh D., Holleitner A. W., and Kotthaus J. P. Micropatterned electrostatic traps for indirect excitons in coupled GaAs quantum wells, *Phys. Rev. B* **76**, 085304 (2007).

[87] Schinner G. J., Schubert E., Stallhofer M. P., Kotthaus J. P., Schuh D., Rai A. K., Reuter D., Wieck A. D., and Govorov A. O. Electrostatically trapping indirect excitons in coupled $In_xGa_{1x}As$ quantum wells, *Phys. Rev. B* **83**, 165308 (2011).

[88] High A. A., Leonard J. R., Remeika M., Butov L. V., Hanson M., and Gossard A. C. Condensation of excitons in a trap, *Nano Lett.* **12**, 2605 (2012).

[89] Alloing M., Lemaître A., Galopin E., and Dubin F. Nonlinear dynamics and inner-ring photoluminescence pattern of indirect excitons, *Phys. Rev. B* **85**, 245106 (2012).

[90] Hagn M., Zrenner A., Böhm G., and Weimann G. Electricfieldinduced exciton transport in coupled quantum well structures, *Appl. Phys. Lett.* **67**, 232 (1995).

[91] Gärtner A., Holleitner A. W., Kotthaus J. P., and Schuh D. Drift mobility of long-living excitons in coupled GaAs quantum wells, *Appl. Phys. Lett.* **89**, 052108 (2006).

[92] Zimmermann S., Govorov A. O., Hansen W., Kotthaus J. P., Bichler M., and Wegscheider W. Lateral superlattices as voltage-controlled traps for excitons, *Phys. Rev. B* **56**, 13414 (1997).

[93] Zimmermann S., Schedelbeck G., Govorov A. O., Wixforth A., Kotthaus J. P., Bichler M., Wegscheider W., and Abstreiter G. Spatially resolved exciton trapping in a voltage-controlled lateral superlattice, *Appl. Phys. Lett.* **73**, 154 (1998).

[94] Remeika M., Fogler M. M., Butov L. V., Hanson M., and Gossard A. C. Two-dimensional electrostatic lattices for indirect excitons, *Appl. Phys. Lett.* **100**, 061103 (2012).

[95] High A. A., Hammack A. T., Butov L. V., Hanson M., and Gossard A. C. Exciton optoelectronic transistor, *Optics Lett.* **32**, 2466 (2007).

[96] High A. A., Novitskaya E. E., Butov L. V., Hanson M., and Gossard A. C. Control of exciton fluxes in an excitonic integrated circuit, *Science* **321**, 229 (2008).

[97] Grosso G., Graves J., Hammack A. T., High A. A., Butov L. V., Hanson M., and Gossard A. C. Excitonic switches operating at around 100 K, *Nat. Photonics* **3**, 577 (2009).

[98] Winbow A. G., Leonard J. R., Remeika M., Kuznetsova Y. Y., High A. A., Hammack A. T., Butov L. V., Wilkes J., Guenther A. A., Ivanov A. L., Hanson M., and Gossard A. C. Electrostatic conveyer for excitons, *Phys. Rev. Lett.* **106**, 196806 (2011).

[99] Zrenner A., Butov L. V., Hagn M., Abstreiter G., Böhm G., and Weimann G. Quantum dots formed by interface fluctuations in AlAs/GaAs coupled quantum well structures, *Phys. Rev. Lett.* **72**, 3382 (1994).

[100] Butov L. V., Lai C. W., Ivanov A. L., Gossard A. C., and Chemla D. S. Towards Bose-Einstein condensation of excitons in potential traps, *Nature* **417**, 47 (2002).

[101] Trauernicht D. P., Mysyrowicz A., and Wolfe J. P. Strain confinement and thermodynamics of free excitons in a direct-gap semiconductor, *Phys. Rev. B* **28**, 3590 (1983).

[102] Kash K., Worlock J. M., Sturge M. D., Grabbe P., Harbison J. P., Scherer A., and Lin P. S. D. Straininduced lateral confinement of excitons in GaAsAlGaAs quantum well microstructures, *Appl. Phys. Lett.* **53**, 782 (1988).

[103] Negoita V., Snoke D. W., and Eberl K. Harmonic-potential traps for indirect excitons in coupled quantum wells, *Phys. Rev. B* **60**, 2661 (1999).

[104] Naka N. and Nagasawa N. Bosonic stimulation of cold excitons in a harmonic potential trap in Cu_2O, *J. Lumin.* **112**, 11 (2005).

[105] Vörös Z., Snoke D. W., Pfeiffer L., and West K. Trapping excitons in a two-dimensional in-plane harmonic potential: Experimental evidence for equilibration of indirect excitons, *Phys. Rev. Lett.* **97**, 016803 (2006)

[106] Yoshioka K., Chae E., and Kuwata-Gonokami M. Transition to a BoseEinstein condensate and relaxation explosion of excitons at sub-Kelvin temperatures, *Nat. Commun.* **2**, 328 (2011).

[107] Hammack A. T., Griswold M., Butov L. V., Smallwood L. E., Ivanov A. L., and Gossard A. C. Trapping of cold excitons in quantum well structures with laser light, *Phys. Rev. Lett.* **96**, 227402 (2006).

[108] Alloing M., Lemaître A., Galopin E., and Dubin F. Optically programmable excitonic traps, *Sci. Rep.* **3**, 1578 (2013).

[109] Christianen P. C. M., Piazza F., Lok J. G. S., Maan J. C., and van der Vleuten W. Magnetic trap for excitons, *Physica B* **251**, 624 (1998).

[110] Butov L. V., Ivanov A. L., İmamoğlu A., Littlewood P. B., Shashkin A. A., Dolgopolov V. T., Campman K. L., and Gossard A. C. Stimulated scattering of indirect excitons in coupled quantum wells: Signature of a degenerate Bose-gas of excitons, *Phys. Rev. Lett.* **86**, 5608 (2001).

[111] Krivolapchuk V. V., Moskalenko E. S., Zhmodikov A. L., Cheng T. S., and Foxon C. T. Collective properties of spatially indirect excitons in asymmetric GaAs/AlGaAs double quantum wells, *Solid State Commun.* **111**, 49 (1999).

[112] Kuz'min R. V., Krivolapchuk V. V., Moskalenko E. S., and Mezdrogina M. M. Radiation intensity fluctuations of an exciton Bose condensate in GaAs/$Al_{0.33}Ga_{0.67}$As double quantum wells, *Fiz. Tverd. Tela.* **52**, 1184 (2010). [Sov. Phys. Solid State **52**, 1260 (2010)].

[113] Larionov A. V., Timofeev V. B., Hvam J., and Soerensen C. Collective behavior of interwell excitons in GaAs/AlGaAs double quantum wells, *JETP Lett.* **71**, 117 (2000).

[114] Larionov A. V., Timofeev V. B., Hvam J., and Soerensen K. Collective state of interwell excitons in GaAs/AlGaAs double quantum wells under pulse resonance excitation, *JETP Lett.* **75**, 200 (2002).

[115] Butov L. V. and Filin A. I. Anomalous transport and luminescence of indirect excitons in AlAs/GaAs coupled quantum wells as evidence for exciton condensation, *Phys. Rev. B* **58**, 1980 (1998).

[116] Larionov A. V., Timofeev V. B., Ni P. A., Dubonos S. V., Hvam I., and Soerensen K. Bose condensation of interwell excitons in double quantum wells, *JETP Lett.* **75**, 570 (2002).

[117] Snoke D., Wolfe J. P., and Mysyrowicz A. Quantum saturation of a Bose gas: Excitons in Cu_2O, *Phys. Rev. Lett.* **59**, 827 (1987).

[118] Lin J. L. and Wolfe J. P. Bose-Einstein condensation of paraexcitons in stressed Cu_2O, *Phys. Rev. Lett.* **71**, 1222 (1993).

[119] Fukuzawa T., Mendez E. E., and Hong J. M. Phase transition of an exciton system in GaAs coupled quantum wells, *Phys. Rev. Lett.* **64**, 3066 (1990).

[120] O'Hara K. E., Súilleabhá in L. Ó., and Wolfe J. P. Strong nonradiative recombination of excitons in Cu_2O and its impact on Bose-Einstein statistics, *Phys. Rev. B* **60**, 10565 (1999).

[121] O'Hara K. E. and Wolfe J. P. Relaxation kinetics of excitons in cuprous oxide, *Phys. Rev. B* **62**, 12909 (2000).

[122] Kash J. A., Zachau M., Mendez E. E., Hong J. M., and Fukuzawa T. Fermi-Dirac distribution of excitons in coupled quantum wells, *Phys. Rev. Lett.* **66**, 2247 (1991).

[123] Yang S., Hammack A. T., Fogler M. M., Butov L. V., and Gossard A. C. Coherence length of cold exciton gases in coupled quantum wells, *Phys. Rev. Lett.* **97**, 187402 (2006).

[124] Semkat D., Sobkowiak S., Manzke G., and Stolz H. Comment on "Condensation of excitons in a trap", *Nano Lett.* **12**, 5055 (2012).

[125] High A. A., Leonard J. R., Remeika M., Butov L. V., Hanson M., and Gossard A. C. Reply to "Comment on 'Condensation of excitons in a trap"', *Nano Lett.* **12**, 5422 (2012).

[126] Alloing M., Fuster D., Gonzalez Y., Gonzalez L., and Dubin F. Observation of macroscopic coherence in self-organized dipolar excitons, arXiv:1210.3176 (2012).

[127] Östreich T., Portengen T., and Sham L. J. Second-order optical response from a Bose-Einstein condensate of excitons, *Solid State Commun.* **100**, 325 (1996).

[128] Fernández-Rossier J., Tejedor C., and Merlin R. Coherent-light emission from exciton condensates in semiconductor quantum wells, *Solid State Commun.* **108**, 473 (1998).

[129] Olaya-Castro A., Rodríguez F. J., Quiroga L., and Tejedor C. Restrictions on the coherence of the ultrafast optical emission from an electron-hole-pair condensate, *Phys. Rev. Lett.* **87**, 246403 (2001).

[130] Keeling J., Levitov L. S., and Littlewood P. B. Angular distribution of photoluminescence as a probe of Bose condensation of trapped excitons, *Phys. Rev. Lett.* **92**, 176402 (2004).

[131] Zimmermann R. Probing exciton condensation by speckled emission, *Solid State Commun.* **134**, 43 (2005).

[132] Levitov L. S., Simons B. D., and Butov L. V. Pattern formation as a signature of quantum degeneracy in a cold exciton system, *Phys. Rev. Lett.* **94**, 176404 (2005).

[133] Maialle M. Z., de Andrada e Silva E. A., and Sham L. J. Exciton spin dynamics in quantum wells, *Phys. Rev. B* **47**, 15776 (1993).

[134] Fernández-Rossier J. and Tejedor C. Spin degree of freedom in two dimensional exciton condensates, *Phys. Rev. Lett.* **78**, 4809 (1997).

[135] Yao W. and Niu Q. Berry phase effect on the exciton transport and on the exciton Bose-Einstein condensate, *Phys. Rev. Lett.* **101**, 106401 (2008).

[136] Combescot M., Betbeder-Matibet O., and Combescot R. Bose-Einstein condensation in semiconductors: The key role of dark excitons, *Phys. Rev. Lett.* **99**, 176403 (2007).

[137] Combescot M., Moore M. G., and Piermarocchi C. Optical traps for dark excitons, *Phys. Rev. Lett.* **106**, 206404 (2011).

[138] Hakioğlu T. and Şahin M. Excitonic condensation under spin-orbit coupling and BEC-BCS crossover, *Phys. Rev. Lett.* **98**, 166405 (2007).

[139] Can M. Ali and Hakioğlu T. Unconventional pairing in excitonic condensates under spin-orbit coupling, *Phys. Rev. Lett.* **103**, 086404 (2009)

[140] Wu C., Mondragon-Shem I., and Zhou X.-F. Unconventional Bose-Einstein condensations from spin-orbit coupling, *Chin. Phys. Lett.* **28**, 097102 (2011).

[141] Shim Y.-P. and MacDonald A. H. Spin-orbit interactions in bilayer exciton-condensate ferromagnets, *Phys. Rev. B* **79**, 235329 (2009).

[142] Leonard J. R., Kuznetsova Y. Y., Yang S., Butov L. V., Ostatnický T., Kavokin A., and Gossard A. C. Spin transport of excitons, *Nano Lett.* **9**, 4204 (2009).

[143] Kowalik-Seidl K., Vögele X. P., Rimpfl B. N., Manus S., Kotthaus J. P., Schuh D., Wegscheider W., and Holleitner A. W. Long exciton spin relaxation in coupled quantum wells, *Appl. Phys. Lett.* **97**, 011104 (2010).

[144] Bucher B., Steiner P., and Wachter P. Excitonic insulator phase in $TmSe_{0.45}Te_{0.55}$, *Phys. Rev. Lett.* **67**, 2717 (1991).

[145] Wachter P., Jung A., and Steiner P. Pressure-driven metal-insulator transition in La-doped SmS: Excitonic condensation, *Phys. Rev. B* **51**, 5542 (1995).

[146] Wachter P. The discovery of excitonium, *J. Alloys Compounds*, **225**, 133 (1995).

[147] Jansen H. J. F., Freeman A. J., and Monnier R. Local-density theory of mixed-valence TmSe and the valence transition in Tm chalcogenides, *Phys. Rev. B* **31**, 4092 (1985).

[148] Wachter P., Bucher B., and Malar J. Possibility of a superfluid phase in a Bose condensed excitonic state, *Phys. Rev. B* **69**, 094502 (2004).

[149] Bronold F. X. and Fehske H. Possibility of an excitonic insulator at the semiconductor-semimetal transition, *Phys. Rev. B* **74**, 165107 (2006).

[150] Bronold F. X., Fehske H., and Röpke G. Excitonic versus electron-hole liquid phases in Tm[Se,Te] compounds, *J. Phys. Soc. Jpn.* **76**,(Supplement A), 27 (2007)

[151] Zenker B., Ihle D., Bronold F. X., and Fehske H. Electron-hole pair condensation at the semimetal-semiconductor transition: A BCS-BEC crossover scenario, *Phys. Rev. B* **85**, 121102(R) (2012).

[152] Di Salvo F. J., Moncton D. E., and Waszczak J. V. Electronic properties and superlattice formation in the semimetal $TiSe_2$ *Phys. Rev. B* **14**, 4321 (1976).

[153] Wilson J. A. Concerning the semimetallic characters of TiS_2 and $TiSe_2$, *Solid State Commun.*, **22**, 551 (1977).

[154] Traum M. M., Margaritondo G., Smith N. V., Rowe J. E., and Di Salvo F. J. TiSe2: Semiconductor semimetal, or excitonic insulator, *Phys. Rev. B* **17**, 1836 (1978).

[155] Margaritondo G., Bertoni C. M., Weaver J. H., Lévy F., Stoffel N. G., and Katnani A. D. Density-of-states changes near the Fermi level and the lattice instability in $TiSe_2$, *Phys. Rev. B* **23**, 3765 (1981).

[156] Stoffel N. G., Lévy F., Bertoni C. M., and Margaritondo G. Direct evidence for d-band involvement in the $TiSe_2$ phase transition, *Solid State Commun.* **41**, 53 (1982).

[157] Anderson O., Manzke R., and Skibowski M. Three-dimensional and relativistic effects in layered 1*T* -$TiSe_2$, *Phys. Rev. Lett.* **55**, 2188 (1985).

[158] Pillo T., Hayoz J., Berger H., Lévy F., Schlapbach L., and Aebi P. Photoemission of bands above the Fermi level: The excitonic insulator phase transition in 1*T*-$TiSe_2$, *Phys. Rev. B* **61**, 16213 (2000).

[159] Kidd T. E., Miller T., Chou M. Y., and Chiang T.-C. Electron-hole coupling and the charge density wave transition in $TiSe_2$, *Phys. Rev. Lett.* **88**, 226402 (2002).

[160] Cercellier H., Monney C., Clerc F., Battaglia C., Despont L., Garnier M. G., Beck H., Aebi P., Patthey L., Berger H., and Forró L. Evidence for an excitonic insulator phase in 1*T*-$TiSe_2$, *Phys. Rev. Lett.* **99**, 146403 (2007).

[161] Rasch J. C. E., Stemmler T., Müller B., Dudy L., and Manzke R. 1*T*-$TiSe_2$: Semimetal or semiconductor? *Phys. Rev. Lett.* **101**, 237602 (2008).

[162] Monney C., Schwier E. F., Garnier M. G., Mariotti N., Didiot C., Beck H., Aebi P., Cercellier H., Marcus J., Battaglia C., Berger H., and Titov A. N. Temperature-dependent photoemission on 1*T*-$TiSe_2$: Interpretation within the exciton condensate phase model, *Phys. Rev. B* **81**, 155104 (2010).

[163] van Wezel J., Nahai-Williamson P., and Saxena S. S. An alternative interpretation of recent ARPES measurements on $TiSe_2$, *Europhys. Lett.* **89**, 47004 (2010).

[164] Monney C., Battaglia C., Cercellier H., Aebi P., and Beck H. Exciton condensation driving the periodic lattice distortion of 1*T*-$TiSe_2$, *Phys. Rev. Lett.* **106**, 106404 (2011).

[165] May M. M., Brabetz C., Janowitz C., and Manzke R. Charge-density-wave phase of 1*T* -$TiSe_2$: The influence of conduction band population, *Phys. Rev. Lett.* **107**, 176405 (2011).

[166] Cazzaniga M., Cercellier H., Holzmann M., Monney C., Aebi P., Onida G., and Olevano V. Ab initio many-body effects in $TiSe_2$: A possible excitonic insulator scenario from GW band-shape renormalization, *Phys. Rev. B* **85**, 195111 (2012).

[167] Wakisaka Y., Sudayama T., Takubo K., Mizokawa T., Arita M., Namatame H., Taniguchi M., Katayama N., Nohara M., and Takagi H. Excitonic insulator state in Ta_2NiSe_5 probed by photoemission spectroscopy, *Phys. Rev. Lett.* **103**, 026402 (2009).

[168] Taraphder A., Koley S., Vidhyadhiraja N. S., and Laad M. S. Preformed excitonic liquid route to a charge density wave in 2*H*-$TaSe_2$, *Phys. Rev. Lett.* **106**, 236405 (2011).

[169] Bascones E., Burkov A. A., and MacDonald A. H. Theory of ferromagnetism in doped excitonic condensates, *Phys. Rev. Lett.* **89**, 086401 (2002).

[170] Taraphder A., Laad M. S., Craco L., and Yaresko A. N. GdI2: A new ferromagnetic excitonic solid? *Phys. Rev. Lett.* **101**, 136410 (2008).

[171] Rossnagel K. On the origin of charge-density waves in select layered transition-metal dichalcogenides, *J. Phys.: Condens. Matter* **23**, 213001 (2011).

[172] Grüner G. *Density Waves in Solids*. Westview Press, Boulder, CO (2000).

[173] Rohwer T., Hellmann S., Wiesenmayer M., Sohrt C., Stange A., Slomski B., Carr A., Liu Y., Avila L. M., Kalläne M., Mathias S., Kipp L., Rossnagel K., and Bauer

M. Collapse of long-range charge order tracked by time-resolved photoemission at high momenta, *Nature* **471**, 490 (2011).

[174] Hellmann S., Rohwer T., Kalläne M., Hanff K., Sohrt C., Stange A., Carr A., Murname M. M., Kapteyn H. C., Kipp L., Bauer M., and Rossnagel K. Time-domain classification of charge-density-wave insulators, *Nat. Commun.* **3**, 1069 (2012).

[175] Aeppli G. and Fisk Z. Kondo insulators, *Comments Condens. Matter Phys.* **16**, 155 (1992).

[176] Lee P. A., Rice T. M., Serene J. W., Sham L. J., and Wilkins J. W. Theories of heavy-fermion systems, *Comments Condens. Matter Phys.* **12**, 99 (1986).

[177] Falicov L. M. and Kimball J. C. Simple model for semiconductor-metal transitions: SmB_6 and transition-metal oxides, *Phys. Rev. Lett.* **22**, 997 (1969).

[178] Portengen T., Östreich Th., and Sham L. J. Linear and nonlinear optical characteristics of the Falicov-Kimball model, *Phys. Rev. Lett.* **76**, 3384 (1996).

[179] Rontani M. and Sham L. J. Thermoelectric properties of junctions between metal and strongly correlated semiconductor, *Appl. Phys. Lett.* **77**, 3033 (2000).

[180] Rontani M. and Sham L. J, *Properties and Applications of Thermoelectric Materials*, p. 193, NATO Science for Peace and Security Series B: Physics and Biophysics Springer, Dordrecht, The Netherlands (2009).

[181] Portengen T., Östreich Th., and Sham L. J. Theory of electronic ferroelectricity, *Phys. Rev. B* **54**, 17452 (1996).

[182] Kittel C, *Introduction to Solid State Physics*, John Wiley, New York. (1986).

[183] Wachter P. and Travaglini G. Intermediate valence and the hybridization model: A study on SmB_6 "gold" SmS and YbB_{12}, *J. Magn. Magn. Mater.* **47–48**, 423 (1985).

[184] Glushkov V. V., Demishev S. V., Ignatov M. I., Paderno Y. B., Shitsevalova N. Y., Kuznetsov A. V., Churkin O. A., Sluchanko D. N., and Sluchanko N. E. An observation of electron phase transition in SmB_6 at low temperatures, *J. Solid State Chem.* **179**, 2871 (2006).

[185] Duan J.-M., Arovas D. P., and Sham L. J. Kondo insulator: p-wave Bose condensate of excitons, *Phys. Rev. Lett.* **79**, 2097 (1997).

[186] Bulou A., Rousseau M., and Nouet J. Ferroelastic phase transitions and related phenomena, *Key Eng. Mater.* **68**, 133 (1992).

[187] Sivan U., Solomon P. M., and Shtrikman H. Coupled electron-hole transport, *Phys. Rev. Lett.* **68**, 1196 (1992).

[188] Kane B. E., Eisenstein J. P., Wegscheider W., Pfeiffer L. N., and West K. W. Separately contacted electronhole double layer in a GaAs/Al_xGa_{1x}As heterostructure, *Appl. Phys. Lett.* **65**, 3266 (1994).

[189] Pohlt M., Lynass M., Lok J. G. S., Dietsche W., von Klitzing K., Eberl K., and Mühle R. Closely spaced and separately contacted two-dimensional electron and hole gases by in situ focused-ion implantation, *Appl. Phys. Lett.* **80**, 2105 (2002).

[190] Keogh J. A., Das Gupta K., Beere H. E., Ritchie D. A., and Pepper M. Fabrication of closely spaced, independently contacted electron-hole bilayers in GaAs-AlGaAs heterostructures, *Appl. Phys. Lett.* **87**, 202104 (2005).

[191] Prunnila M., Laakso S. J., Kivioja J. M., and Ahopelto J. Electrons and holes in Si quantum well: A room-temperature transport and drag resistance study, *Appl. Phys. Lett.* **93**, 112113 (2008).

[192] Takashina K., Nishiguchi K., Ono Y., Fujiwara A., Fujisawa T., Hirayama Y., and Muraki K. Electrons and holes in a 40 nm thick silicon slab at cryogenic temperatures, *Appl. Phys. Lett.* **94**, 142104 (2009).

[193] Das Gupta K., Croxall A. F., Waldie J. Nicoll C. A., Beere H. E., Farrer I., Ritchie D. A., and Pepper M. Experimental progress towards probing the ground state of an electron-hole bilayer by low-temperature transport, *Adv. in Condens. Matter Phys.* **2011**, 727958 (2011).

[194] Vignale G. and MacDonald A. H. Drag in paired electron-hole layers, *Phys. Rev. Lett.* **76**, 2786 (1996).

[195] Hu B. Y.-K. Prospecting for the superfluid transition in electron-hole coupled quantum wells using Coulomb drag, *Phys. Rev. Lett.* **85**, 820 (2000).

[196] Joglekar Y. N., Balatsky A. V., and Lilly M. P. Excitonic condensate and quasiparticle transport in electron-hole bilayer systems, *Phys. Rev. B* **72**, 205313 (2005).

[197] Croxall A. F., Gupta K. Das, Nicoll C. A., Thangaraj M., Beere H. E., Farrer I., Richtie D. A., and Pepper M. Anomalous Coulomb drag in electron-hole bilayers, *Phys. Rev. Lett.* **101**, 246801 (2008).

[198] Seamons J. A., Morath C. P., Reno J. L., and Lilly M. P. Coulomb drag in the exciton regime in electron-hole bilayers, *Phys. Rev. Lett.* **102**, 026804 (2009).

[199] Croxall A. F., Das Gupta K., Nicoll C. A., Thangaraj M., Beere H. E., Farrer I., Ritchie D. A., and Pepper M. Possible effect of collective modes in zero magnetic field transport in an electron-hole bilayer, *Phys. Rev. B* **80**, 125323 (2009).

[200] Eisenstein J. P. Evidence for spontaneous interlayer phase coherence in a bilayer quantum Hall exciton condensate, *Solid State Commun.* **127**, 123 (2003).

[201] Eisenstein J. P. and MacDonald A. H. BoseEinstein condensation of excitons in bilayer electron systems, *Nature* **432**, 691 (2004).

[202] Tutuc E. and Shayegan M. Charge neutral counterflow transport at filling factor 1 in GaAs hole bilayers, *Solid State Commun.* **144**, 405 (2007).

[203] Kuramoto Y. and Horie C. Two-dimensional excitonic phase in strong magnetic fields, *Solid State Commun.* **25**, 713 (1978).

[204] Yoshioka D. and MacDonald A. H. Double quantum well electron-hole systems in strong magnetic fields, *J. Phys. Soc. Jpn.* **59**, 4211 (1990).

[205] MacDonald A. H. and Rezayi E. H. Fractional quantum Hall effect in a two-dimensional electron-hole fluid, *Phys. Rev. B* **42**, 3224 (1990).

[206] Spielman I. B., Eisenstein J. P., Pfeiffer L. N., and West K. W. Resonantly enhanced tunneling in a double layer quantum Hall ferromagnet, *Phys. Rev. Lett.* **84**, 5808 (2000).

[207] Su J.-J. and MacDonald A. H. How to make a bilayer exciton condensate flow, *Nat. Phys.* **4**, 799 (2008).

[208] Kellog M., Eisenstein J. P., Pfeiffer L. N., and West K. W. Vanishing Hall resistance at high magnetic field in a double-layer two-dimensional electron system, *Phys. Rev. Lett.* **93**, 036801 (2004).

[209] Tutuc E., Shayegan M., and Huse D. A. Counterflow measurements in strongly correlated GaAs hole bilayers: Evidence for electron-hole pairing, *Phys. Rev. Lett.* **93**, 036802 (2004).

[210] Wiersma R. D., Lok J. G. S., Kraus S., Dietsche W., von Klitzing K., Schuh D., Bichler M., Tranitz H.-P., and Wegscheider W. Activated transport in the

separate layers that form the $\nu_T = 1$ exciton condensate, *Phys. Rev. Lett.* **93**, 266805 (2004).

[211] Tiemann L., Lok J. G. S., Dietsche W., von Klitzing K., Muraki K., Schuh D., and Wegscheider W. Exciton condensate at a total filling factor of one in Corbino two-dimensional electron bilayers, *Phys. Rev. B* **77**, 033306 (2008).

[212] Tiemann L., Dietsche W., Hauser M., and von Klitzing K. Critical tunneling currents in the regime of bilayer excitons, *New J. Phys.* **10**, 045018 (2008).

[213] Finck A. D. K., Eisenstein J. P., Pfeiffer L. N., and West K. W. Exciton transport and Andreev reflection in a bilayer quantum Hall system, *Phys. Rev. Lett.* **106**, 236807 (2011).

[214] Nandi A., Finck A. D. K., Eisenstein J. P., Pfeiffer L. N., and West K. W. Exciton condensation and perfect Coulomb drag, *Nature*, **488**, 481 (2012).

[215] Spielman I. B., Eisenstein J. P., Pfeiffer L. N., and West K. W. Observation of a linearly dispersing collective mode in a quantum Hall ferromagnet, *Phys. Rev. Lett.* **87**, 036803 (2001).

[216] Giudici P., Muraki K., Kumada N., and Fujisawa T. Intrinsic gap and exciton condensation in the $\nu_T = 1$ bilayer system, *Phys. Rev. Lett.* **104**, 056802 (2010).

[217] Luin S., Pellegrini V., Pinczuk A., Dennis B. S., Pfeiffer L. N., and West K. W. Observation of soft magnetorotons in bilayer quantum Hall ferromagnets, *Phys. Rev. Lett.* **90**, 236802 (2003).

[218] Karmakar B., Pellegrini V., Pinczuk A., Pfeiffer L. N., and West K. W. First-order quantum phase transition of excitons in quantum Hall bilayers, *Phys. Rev. Lett.* **102**, 036802 (2009).

[219] Balatsky A. V., Joglekar Y. N., and Littlewood P. B. Dipolar superfluidity in electron-hole bilayer systems, *Phys. Rev. Lett.* **93**, 266801 (2004).

[220] Sonin E. B. Gauge-field rotation of an electrically polarized Bose condensate by a radial magnetic field, *Phys. Rev. Lett.* **102**, 106407 (2009).

[221] Eastham P. R., Cooper N. R., and Lee D. K. K. Diamagnetism and flux creep in bilayer exciton superfluids, *Phys. Rev. B* **85**, 165320 (2012).

[222] Dubi Y. and Balatsky A. V. Impurity-induced bound states and proximity effect in a bilayer exciton condensate, *Phys. Rev. Lett.* **104**, 166802 (2010).

[223] Dolcini F., Rainis D., Taddei F., Polini M., Fazio R., and MacDonald A. H. Blockade and counterflow supercurrent in exciton-condensate Josephson junctions, *Phys. Rev. Lett.* **104**, 027004 (2010).

[224] Peotta S., Gibertini M., Dolcini F., Taddei F., Polini M., Ioffe L. B., Fazio R., and MacDonald A. H. Josephson current in a four-terminal superconductor/exciton-condensate/superconductor system, *Phys. Rev. B* **84**, 184528 (2011).

[225] Soller H., Dolcini F., and Komnik A. Nanotransformation and current fluctuations in exciton condensate junctions, *Phys. Rev. Lett.* **108**, 156401 (2012).

[226] Chen X. M. and Quinn J. J. Excitonic charge-density-wave instability of spatially separated electron-hole layers in strong magnetic fields, *Phys. Rev. Lett.*, **67**, 895 (1991).

[227] Geim A. K. and Novoselov K. S. The rise of graphene, *Nat. Mat.* **6**, 183 (2007).

[228] Castro Neto A. H., Guinea F., Peres N. M. R., Novoselov K. S., and Geim A. K. The electronic properties of graphene, *Rev. Mod. Phys.* **81**, 109 (2009)

[229] Das Sarma S., Adam S., Hwang E. H., and Rossi E. Electronic transport in two-dimensional graphene, *Rev. Mod. Phys.* **83**, 407 (2011).

[230] Kotov V. N., Uchoa B., Pereira V. M., Guinea F., and Castro Neto A. H. Electron-electron interactions in graphene: Current status and perspectives, *Rev. Mod. Phys.* **84**, 1067 (2012).

[231] Grosso G. and Pastori Parravicini G. *Solid State Physics* (1st edn), Academic Press, San Diego (2000).

[232] Khveshchenko D. V. Ghost excitonic insulator transition in layered graphite, *Phys. Rev. Lett.* **87**, 246802 (2001).

[233] Vafek O. and Case M. J. Renormalization group approach to two-dimensional Coulomb interacting Dirac fermions with random gauge potential, *Phys. Rev. B* **77**, 033410 (2008).

[234] Drut J. E. and Lände T. A. Is graphene in vacuum an insulator? *Phys. Rev. Lett.* **102**, 026802 (2009).

[235] Gamayun O. V., Gorbar E. V., and Gusynin V. P. Supercritical Coulomb center and excitonic instability in graphene, *Phys. Rev. B* **80**, 165429 (2009).

[236] González J. Electron self-energy effects on chiral symmetry breaking in graphene, *Phys. Rev. B* **85**, 085420 (2012).

[237] Wang J.-R. and Liu G.-Z. Absence of dynamical gap generation in suspended graphene, *New J. Phys.* **14**, 043036 (2012).

[238] Castro Neto A. H. Pauling s dreams for graphene, *Physics* **2**, 30 (2009).

[239] Semenoff G. W. Chiral symmetry breaking in graphene, *Physica Scripta* **T146**, 014016 (2012).

[240] Uchoa B., Reed J. P., Gan Y., Joe Y. II, Fradkin E., Abbamonte P., and Casa D. The electron many-body problem in graphene, *Phys. Scripta* **T146**, 014014 (2012).

[241] Elias D. C., Gorbachev R. V., Mayorov A. S., Morozov S. V., Zhukov A. A., Blake P., Ponomarenko L. A., Grigorieva I. V., Novoselov K. S., Guinea F., and Geim A. K. Dirac cones reshaped by interaction effects in suspended graphene, *Nat. Phys.* **7**, 701 (2011).

[242] Bostwick A., Speck F., Seyller T., Horn K., Polini M., Asgari R., MacDonald A. H., and Rotenberg E. Observation of plasmarons in quasi-freestanding doped graphene, *Science* **328**, 999 (2010).

[243] Du X., Skachko I., Duerr F., Luican A., and Andrei E. Y. Fractional quantum Hall effect and insulating phase of Dirac electrons in graphene, *Nature* **462**, 192 (2009).

[244] Bolotin K. I., Ghahari F., Shulman M. D., Stormer H. L., and Kim P. Observation of the fractional quantum Hall effect in graphene, *Nature* **462**, 196 (2009).

[245] Lozovik Y. E. and Sokolik A. A. Electron-hole pair condensation in a graphene bilayer, *JETP Lett.* **87**, 55 (2008).

[246] Dillenschneider R. and Han J. H. Exciton formation in graphene bilayer, *Phys. Rev. B* , **78**, 045401 (2008).

[247] Min H., Bistritzer R., Su J.-J., and MacDonald A. H. Room-temperature superfluidity in graphene bilayers, *Phys. Rev. B* **78**, 121401(R) (2008).

[248] Zhang C.-H and Joglekar Y. N. Excitonic condensation of massless fermions in graphene bilayers, *Phys. Rev. B* **77**, 233405 (2008).

[249] Kharitonov M. Y. and Efetov K. B. Electron screening and excitonic condensation in double-layer graphene systems, *Phys. Rev. B* **78**, 241401(R) (2008).

[250] Bistritzer R., Min H., Su J.-J., and MacDonald A. H. Comment on "Electron screening and excitonic condensation in double-layer graphene systems", arXiv:0810.0331 (2008).

[251] Gilbert M. J. and Shumway J. Probing quantum coherent states in bilayer graphene, *J. Comput. Electron.* **8**, 51 (2009).

[252] Kharitonov M. Y. and Efetov K. B. Excitonic condensation in a doublelayer graphene system, *Semicond. Sci. Tech.* **25**, 034004 (2010).

[253] Mink M. P., Stoof H. T. C., Duine R. A., and MacDonald A. H. Influence of remote bands on exciton condensation in double-layer graphene, *Phys. Rev. B* **84**, 155409 (2011).

[254] Lozovik Y. E., Ogarkov S. L., and Sokolik A. A. Condensation of electron-hole pairs in a two-layer graphene system: Correlation effects, *Phys. Rev. B* **86**, 045429 (2012).

[255] Sodemann I., Pesin D. A., and MacDonald A. H. Interaction-enhanced coherence between two-dimensional Dirac layers, *Phys. Rev. B* **85**, 195136 (2012).

[256] Suprunenko Y. F., Cheianov V., and Fal'ko V. I. Phases of the excitonic condensate in two-layer graphene, *Phys. Rev. B* **86**, 155405 (2012).

[257] Phan V.-N and Fehske H. Coulomb interaction effects in graphene bilayers: Electronhole pairing and plasmaron formation, *New. J. Phys.* **14**, 075007 (2012).

[258] Kim S., Jo I., Nah J., Yao Z., Banerjee S. K., and Tutuc E. Coulomb drag of massless fermions in graphene, *Phys. Rev. B* **83**, 161401(R) (2011).

[259] Gorbachev R. V., Geim A. K., Katsnelson M. I., Novoselov K. S., Tudorovskiy T., Grigorieva I. V., MacDonald A. H., Morozov S. V., Watanabe K., Taniguchi T., and Ponomarenko L. A. Strong Coulomb drag and broken symmetry in double-layer graphene, *Nat. Phys.* **8**, 896 (2012).

[260] Min H., Borghi G., Polini M., and MacDonald A. H. Pseudospin magnetism in graphene, *Phys. Rev. B* **77**, 041407(R) (2008).

[261] Nandkishore R. and Levitov L. Dynamical screening and excitonic instability in bilayer graphene, *Phys. Rev. Lett.* **104**, 156803 (2010).

[262] Zhang F., Min H., Polini M., and MacDonald A. H. Spontaneous inversion symmetry breaking in graphene bilayers, *Phys. Rev. B* **81**, 041402(R) (2010).

[263] Guinea F. Peeling back the layers or doubling the stakes? *Physics* **3**, 1 (2010).

[264] Lemonik Y., Aleiner I. L., Toke C., and Fal'ko V. I. Spontaneous symmetry breaking and Lifshitz transition in bilayer graphene, *Phys. Rev. B* **82**, 201408(R) (2010).

[265] Vafek O. and Yang K. Many-body instability of Coulomb interacting bilayer graphene: Renormalization group approach, *Phys. Rev. B* **81**, 041401(R) (2010).

[266] MacDonald A. H., Jung J., and Zhang F. Pseudospin order in monolayer, bilayer and double-layer graphene, *Phys. Scripta* **T146**, 014012 (2012).

[267] Nandkishore R. and Levitov L. Spontaneously ordered states in bilayer graphene, *Physica Scripta* **T146**, 014011 (2012).

[268] Weitz R. T., Allen M. T., Feldman B. E., Martin J., and Yacoby A. Broken-symmetry states in doubly gated suspended bilayer graphene, *Science* **330**, 812 (2010).

[269] Mayorov A. S., Elias D. C., Mucha-Kruczynski M., Gorbachev R. V., Tudorovskiy T., Zhukov A., Morozov S. V., Katsnelson M. I., Fal'ko V. I.,

Geim A. K., and Novoselov K. S. Interaction-driven spectrum reconstruction in bilayer graphene, *Science* **333**, 860 (2011).

[270] Velasco Jr. J., Jing L., Bao W., Lee Y., Kratz P., Aji V., Bockrath M., Lau C. N., Varma C., Stillwell R., Smirnov D., Zhang F., Jung J., and MacDonald A. H. Transport spectroscopy of symmetrybroken insulating states in bilayer graphene, *Nat. Nanotech.* **7**, 156 (2012).

[271] Freitag F., Trbovic J., Weiss M., and Schönenberger C. Spontaneously gapped ground state in suspended bilayer graphene, *Phys. Rev. Lett.* **108**, 076602 (2012).

[272] Saito R., Dresselhaus G., and Dresselhaus M. S. *Physical Properties of Carbon Nanotubes*, Imperial College Press, London (1998).

[273] Jarillo-Herrero P., Sapmaz S., Dekker C., Kouwenhoven L. P., van der Zant H. S. J. Electron–hole symmetry in a semiconducting carbon nanotube quantum dot, *Nature* **429**, 389 (2005).

[274] Ando T. Excitons in carbon nanotubes, *J. Phys. Soc. Jpn*. **66**, 1066 (1997).

[275] Hartmann R. R., Shelykh I. A., Portnoi M. E. Excitons in narrow-gap carbon nanotubes, *Phys. Rev. B* **84**, 035437 (2011).

[276] Rontani M. Anomalous magnetization of a carbon nanotube as an excitonic insulator, arXiv:1405.3108.

[277] Laird E. A., Kuemmeth, F., Steele G., Grove-Rasmussen K., Nygard J., Flensberg K., and Kouwenhoven L. P., Quantum transport in carbon nanotubes, arXiv:1403.6113.

[278] Luttinger J. M. and Kohn W. Motion of electrons and holes in perturbed periodic fields, *Phys. Rev.* **97**, 869 (1955).

[279] Guseĭnov R. R and Keldysh L. V. Nature of the phase transition under the conditions of an "excitonic" instability in the electronic spectrum of a crystal, *Zh. Eksp. i Teor. Fiz.* **63**, 2255 (1972). [Sov. Phys.–JETP **36**, 1193 (1973)].

[280] Abrikosov A. A., Gorkov L. P., and Dzyaloshinski I. E. *Methods of Quantum Field Theory in Statistical Physics*, Dover, New York (1975).

[281] Andreev A. F. Thermal conductivity of the intermediate state of superconductors, *Zh. Eksp. i Teor. Fiz.* **46**, 1823 (1964). [Sov. Phys.–JETP **19**, 1228 (1964)].

[282] Zagoskin A. M. *Quantum Theory of Many-Body Systems*, Springer, New York (NY) (1998).

[283] Sham L. J. and Nakayama M. Effective-mass approximation in the presence of an interface, *Phys. Rev. B* **20**, 734 (1979).

[284] Blonder G. E., Tinkham M., and Klapwijk T. M. Transition from metallic to tunneling regimes in superconducting microconstrictions: Excess current, charge imbalance, and supercurrent conversion, *Phys. Rev. B* **25**, 4515 (1982).

[285] Datta S. *Electronic Transport in Mesoscopic Systems*. Cambridge University Press, Cambridge (UK) (1995).

[286] Ziman J. M. *Electrons and Phonons*. Clarendon Press, Oxford (UK) (1960).

[287] Barone A. and Paterno G, *Physics and Applications of the Josephson Effect*, Wiley, New York (1982).

[288] Avenel O. and Varoquaux E. Observation of singly quantized dissipation events obeying the Josephson frequency relation in the critical flow of superfluid ^{4}He through an aperture, *Phys. Rev. Lett.* **55**, 2704 (1985).

[289] Pereverzev S. V., Loshak A., Backhaus S., Davis J. C., and Packard R. E. Quantum oscillations between two weakly coupled reservoirs of superfluid ^{3}He, *Nature*, **388**, 449 (1997).

[290] Sukhatme K., Mukharsky Y., Chui T., and Pearson D. Observation of the ideal Josephson effect in superfluid ^{4}He *Nature* **411**, 280 (2001).

[291] Cataliotti F. S., Burger S., Fort C., Maddaloni P., Minardi F., Trombettoni A., Smerzi A., and Inguscio M. Josephson junction arrays with Bose-Einstein condensates, *Science* **293**, 843 (2001).

[292] Shin Y., Saba M., Pasquini T. A., Ketterle W., Pritchard D. E., and Leanhardt A. E. Atom interferometry with Bose-Einstein condensates in a double-well potential, *Phys. Rev. Lett.* **92**, 050405 (2004).

[293] Albiez M., Gati R., Fölling J., Hunsmann S., Cristiani M., and Oberthaler M. K. Direct observation of tunneling and nonlinear self-trapping in a single bosonic Josephson junction, *Phys. Rev. Lett.* **95**, 010402 (2005).

[294] Levy S., Lahoud E., Shomroni I., and Steinhauer J. The a.c. and d.c. Josephson effects in a BoseEinstein condensate, *Nature* **449**, 579 (2007).

[295] Wouters M. and Carusotto I. Excitations in a nonequilibrium Bose-Einstein condensate of exciton polaritons, *Phys. Rev. Lett.* **99**, 140402 (2007).

[296] Sarchi D., Carusotto I., Wouters M., and Savona V. Coherent dynamics and parametric instabilities of microcavity polaritons in double-well systems, *Phys. Rev. B* **77**, 125324 (2008).

[297] Shelykh I. A., Solnyshkov D. D., Pavlovic G., and Malpuech G. Josephson effects in condensates of excitons and exciton polaritons, *Phys. Rev. B* **78**, 041302(R) (2008).

[298] Anderson P. W. Considerations on the flow of supefluid helium, *Rev. Mod. Phys.* **38**, 298 (1996).

[299] Leggett A. J. and Sols F. On the concept of spontaneously broken gauge symmetry in condensed matter physics, *Found. Phys.* **21**, 353 (1991).

[300] Smerzi A., Fantoni S., Giovanazzi S., and Shenoy S. R. Quantum coherent atomic tunneling between two trapped Bose-Einstein condensates, *Phys. Rev. Lett.* **79**, 4950 (1997).

[301] Raghavan S., Smerzi A., Fantoni S., and Shenoy S. R. Coherent oscillations between two weakly coupled Bose-Einstein condensates: Josephson effects π oscillations, and macroscopic quantum self-trapping, *Phys. Rev. A* **59**, 620 (1999).

[302] Zapata I., Sols F., and Leggett A. J. Josephson effect between trapped Bose-Einstein condensates, *Phys. Rev. A* **57**, R28 (1998).

[303] Östreich T. and Sham L. J. Collective oscillations driven by correlation in the nonlinear optical regime, *Phys. Rev. Lett.* **83**, 3510 (1999).

[304] Glauber R. J. *Quantum Optics and Electronics*, p. 63. Gordon and Breach, New York (1965).

[305] Andrews M. R., Townsend C. G., Miesner H.-J., Durfee D. S., Kurn D. M., and Ketterle W. Observation of interference between two Bose condensates, *Science* **275**, 637 (1997).

[306] Pitaevskii L. and Stringari S. Thermal vs quantum decoherence in double well trapped Bose-Einstein condensates, *Phys. Rev. Lett.* **87**, 180402 (2001).